



Air-quality implications of widespread adoption of cool roofs on ozone and particulate matter in southern California

Scott A. Epstein^{a,1}, Sang-Mi Lee^a, Aaron S. Katzenstein^a, Marc Carreras-Sospedra^a, Xinqiu Zhang^a, Salvatore C. Farina^a, Pouya Vahmani^b, Philip M. Fine^a, and George Ban-Weiss^b

^aPlanning, Rules, and Area Sources Division, South Coast Air Quality Management District, Diamond Bar, CA 91765; and ^bSonny Astani Department of Civil and Environmental Engineering, University of Southern California, Los Angeles, CA 90089

Edited by Christopher B. Field, Stanford University, Stanford, CA, and approved July 5, 2017 (received for review March 8, 2017)

The installation of roofing materials with increased solar reflectance (i.e., “cool roofs”) can mitigate the urban heat island effect and reduce energy use. In addition, meteorological changes, along with the possibility of enhanced UV reflection from these surfaces, can have complex impacts on ozone and PM_{2.5} concentrations. We aim to evaluate the air-quality impacts of widespread cool-roof installations prescribed by California’s Title 24 building energy efficiency standards within the heavily populated and polluted South Coast Air Basin (SoCAB). Development of a comprehensive rooftop area database and evaluation of spectral reflectance measurements of roofing materials allows us to project potential future changes in solar and UV reflectance for simulations using the Weather Research Forecast and Community Multiscale Air Quality (CMAQ) models. 2012 meteorological simulations indicate a decrease in daily maximum temperatures, daily maximum boundary layer heights, and ventilation coefficients throughout the SoCAB upon widespread installation of cool roofs. CMAQ simulations show significant increases in PM_{2.5} concentrations and policy-relevant design values. Changes in 8-h ozone concentrations depend on the potential change in UV reflectance, ranging from a decrease in population-weighted concentrations when UV reflectance remains unchanged to an increase when changes in UV reflectance are at an upper bound. However, 8-h policy-relevant ozone design values increase in all cases. Although the other benefits of cool roofs could outweigh small air-quality penalties, UV reflectance standards for cool roofing materials could mitigate these negative consequences. Results of this study motivate the careful consideration of future rooftop and pavement solar reflectance modification policies.

urban air quality | albedo | California Title 24 | Los Angeles | urban surface modification

The South Coast Air Basin (SoCAB) is a region of southern California encompassing Orange County and the urban portions of Los Angeles, San Bernardino, and Riverside counties. With 16.8 million people, the SoCAB is the second most populous urban area in the United States. A fossil-fuel-dependent transit and goods movement infrastructure along with a well-developed industrial presence within the 27,824-km² SoCAB generates significant emissions of oxides of nitrogen (NO_x), volatile organic compounds (VOCs), directly emitted primary particulate matter (PM), and secondary PM precursors. Persistent high-pressure systems, ample photochemistry, infrequent rainfall, and ventilation-inhibiting topography also contribute to severe air-quality problems. The SoCAB currently does not attain federal air-quality standards for 8-h O₃, 1-h O₃, annual-averaged PM_{2.5}, and 24-h PM_{2.5}. Ozone levels within the SoCAB are often the highest in the nation (1).

The hot and sunny conditions typically experienced within the SoCAB make urban surface modification a useful strategy to reduce urban temperatures. Meteorological impacts of roofing materials with enhanced solar reflectance (SR, synonymous with

“albedo”), colloquially referred to as “cool roofs,” are well-studied and indicate several benefits in urban areas. The replacement of darker materials with high-reflectance surfaces within cities can help mitigate the urban heat island effect (2–14). Moreover, meteorological modeling suggests that the deployment of cool roofs will reduce afternoon summertime temperatures, leading to reduced cooling energy demands, resulting in a curtailment of greenhouse gas emissions (15, 16) in most urban areas. Cool roofs will also lower the Earth’s radiative forcing by increasing the global albedo (17–19), although impacts on global climate remain unsettled in the literature (20), with recent research suggesting effects are negligible (4).

Cool roofs can affect air quality through several mechanisms, although there are far fewer studies investigating these effects compared with the wealth of meteorological and climatological studies. Because the air-quality effects of urban surface modification by cool roofs are complex and nonlinear, comprehensive emissions processing, meteorological, and chemical transport models are needed to accurately determine potential impacts on air quality for policy-making purposes. Potential changes in mixing height and ventilation (21) will affect ambient pollutant concentrations. Cool roofs can reduce temperature-dependent emissions of precursors to O₃ and PM in urban areas by lowering ambient temperatures, resulting in a slower rate of VOC evaporation and NO_x emissions (14). In addition, the atmospheric reactions that produce O₃ are slower at lower temperatures. A

Significance

The South Coast Air Basin of California, a region of 16.8 million people, is among the most polluted air basins in the United States. A multidecadal effort to attain federal air-quality standards has led to significant progress, but much more work remains. Are recently implemented statewide building efficiency standards on rooftops counterproductive to these goals? With comprehensive regional models and intensive development of model input parameters, our research has identified the air-quality consequences that are expected to result from these efficiency standards. The results can inform policies to mitigate some air-quality penalties, while preserving the benefits of building efficiency standards. This work also sheds light on potential future policies aimed at reducing urban heating from pavement surfaces.

Author contributions: S.A.E., S.-M.L., A.S.K., P.M.F., and G.B.-W. designed research; S.A.E., M.C.-S., X.Z., S.C.F., P.V., and G.B.-W. performed research; S.A.E. and S.C.F. contributed new reagents/analytic tools; S.A.E. and G.B.-W. analyzed data; and S.A.E. and G.B.-W. wrote the paper.

The authors declare no conflict of interest.

This article is a PNAS Direct Submission.

¹To whom correspondence should be addressed. Email: sepstein@aqmd.gov.

This article contains supporting information online at www.pnas.org/lookup/suppl/doi:10.1073/pnas.1703560114/-DCSupplemental.

Table 1. Current and future SR values corresponding to Title24 categories

Title24 category	Climate zones	Current SR*	Title24 SR	SoCAB area [†] , km ²	Title24 area [‡] , km ²
Nonresidential low slope	All	23	63	262.3	262.3
Nonresidential high slope	All	19	20	96.5	96.5
High-rise low slope residential, hotel, and motel	9–11, 13–15	20	55	16.1	7.6
High-rise high slope residential, hotel, and motel	2–15	14	20	21.7	21.5
Residential low slope	13–15	20	63	67.2	0.7
Residential high slope	10–15	14	20	580.3	150.6

*Calculated from remote sensing measurements in Los Angeles and Long Beach (11, 12), which were applied to all climate zones.

[†]This is the area of each Title24 land-use category in the SoCAB.

[‡]This is the area of each Title24 land-use category in the SoCAB that is in a climate zone affected by Title24 standards.

handful of studies modeled the effect of cool-roof installations on O₃ concentrations during short-term multiday O₃ episodes in the SoCAB (22–26). Population-weighted O₃ exposures were reduced with an increase in urban SR; however, O₃ concentrations in the less-populated eastern SoCAB exhibited O₃ increases. Further increases in surface SR led to smaller net reductions in O₃ because significant weakening of the sea breeze led to reduced vertical mixing.

To the authors' knowledge, all but one (29) of the previous studies investigating the role of cool-roof materials on air quality assume that widespread adoption of cool roofs will not change UV reflectance (UVR) (2, 22–27). Increases in UVR can significantly affect photochemical production of O₃. For example, O₃ concentrations in the Uintah Basin are elevated in the winter during periods of snow cover due to increased UV reflectivity and limited mixing from reduced surface heating (28). Fallmann et al. (29) modified building SR for all urban grid cells in Stuttgart, Germany from 0.2 to 0.7 across all wavelengths. Although this increase in UVR is unrealistically high, the authors saw a significant increase in peak O₃ concentrations during a clear-sky, sunny period, which they attribute to increases in reflected UV radiation.

In this research effort we aim to rigorously evaluate the air-quality effects in the SoCAB of current cool-roof installation policies in California Title 24 Building Energy Efficiency Standards (Title24) (30). Besides O₃, we also focus on PM_{2.5} concentrations, a pollutant that largely drives the health impacts of air pollution in southern California (31) and whose link to cool-roof adoption is not widely studied. With newly analyzed data on the UVR of hundreds of real-world roofing products, we directly evaluate the assumption used in previous studies that standard and cool roofs have nearly the same UVR and then probe the sensitivity of UVR on resulting pollutant concentrations. Rather than focusing on specific air-pollution episodes, we have conducted a collection of comprehensive simulations over an entire calendar year. We developed a high-resolution database of building rooftop areas classified by land-use category to project future SR after full implementation of Title24 standards in the SoCAB. WRF v3.6, a state-of-the-science meteorological model, was used to forecast changes in meteorology induced by cool roofs. The temperature-dependent 2012 SoCAB emissions inventory (1) and a modified version of the state-of-the-science Community Multiscale Air Quality Model (CMAQ version 5.0.2) were then used to project future O₃ and PM_{2.5} concentrations after cool-roof implementation.

Materials and Methods

Projecting Future SR. Determining the effects of Title24 standards on SR requires information on the current SR and the total rooftop area in each Title24 building category. Title24 standards prescribe that new or renovated rooftops meet SR standards that are based on climate zone (*SI Appendix, Fig. S1*) and building type (30) (Table 1). We determined the rooftop area of each Title24 building category in every model grid cell with land-use data for 2012 from the Southern California Association of Governments (SCAG) and building footprint data from the US Army Corps of Engineers (32). See *SI Appendix*.

We used monthly Moderate Resolution Imaging Spectroradiometer (MODIS) measurements of SR (33) to determine base-case values for each 4-km model grid cell. The current SR of rooftops for each Title24 category in the SoCAB was calculated by combining recent aircraft-based remote sensing measurements of rooftops in Los Angeles and Long Beach, CA (8, 9) with SCAG land-use data (Table 1). The projected future building SR, set by the Title24 standards, along with the current building SR, calculated with the remote sensing measurement data, allowed us to determine the expected change in SR in the fraction of each grid cell occupied by buildings and determine the monthly SR for each grid cell if all rooftops meet Title24 standards. Fig. 1A details the calculated change in grid-cell average SR in response to full implementation of Title24 standards.

Projecting UVR for Chemical Transport Modeling. Photolysis reactions are wavelength-dependent (34); therefore, capturing changes in photochemistry from Title24 requires careful consideration of wavelength-dependent reflectances. In situ remote sensing measurements of rooftop UVR are not available. However, several studies measured the wavelength-dependent spectral reflectance of roofing materials (8, 9, 35–37). To bound the possible change in wavelength-dependent reflectance, Fig. 2 presents spectral reflectance measurements (8, 9) for a wide variety of traditional and cool roof

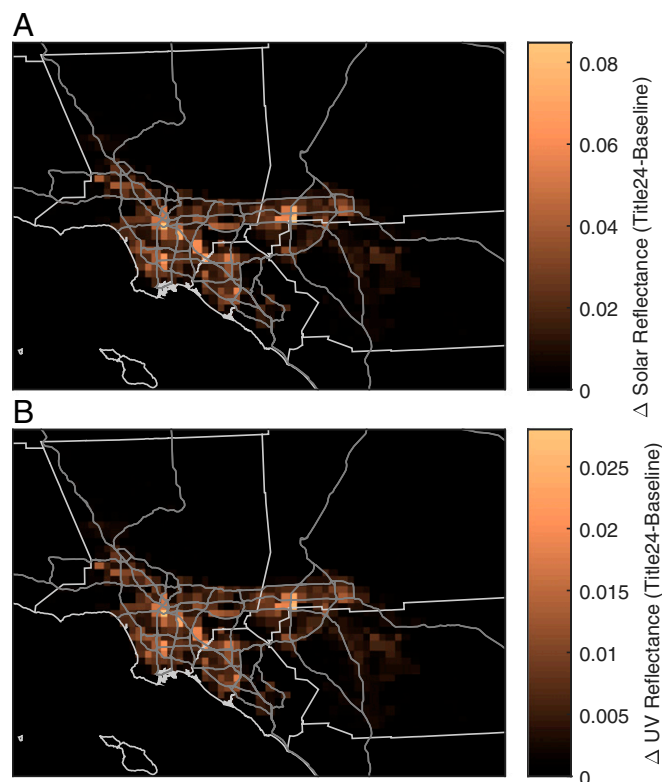


Fig. 1. (A) Change in SR (Title24 – baseline) used for WRF simulations. (B) Maximum possible change in UVR (Title24 – baseline) used for CMAQ simulations.

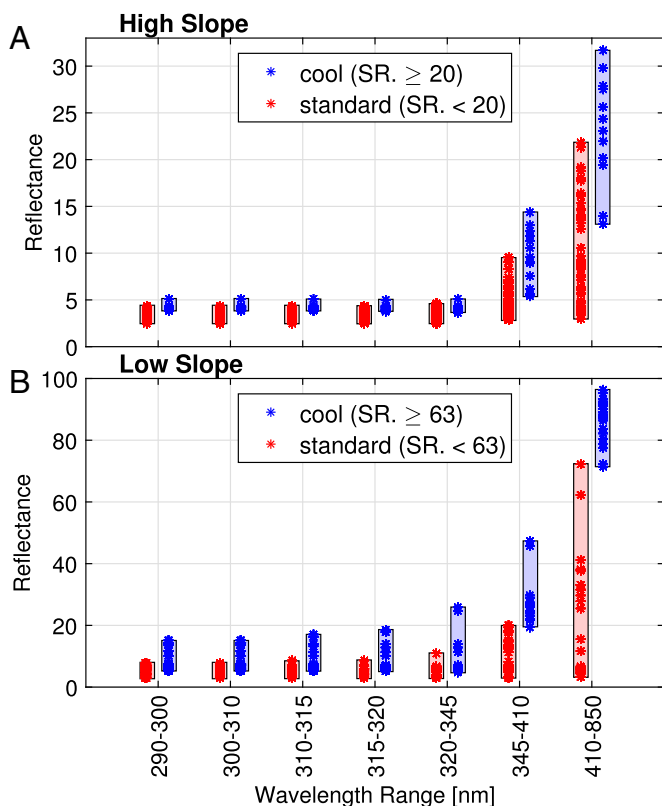


Fig. 2. Range of wavelength-dependent reflectance of cool and standard roofing materials for high-slope (A) and low-slope (B) applications.

materials as a function of wavelength for high slope (Fig. 2A) and low slope (Fig. 2B) roofing materials (*SI Appendix, Table S2*). We define cool roofs, based on Title24 standards, as those with an SR above 0.20 and 0.63 for low-slope and high-slope roofing materials, respectively. To serve as an extreme upper-bound increase in UVR, we set the maximum change in reflectance at each CMAQ wavelength range to be the largest difference between the cool and standard roofing materials (Fig. 1B) and applied these differences to each of the Title24 categories based on their corresponding area in each grid cell. Projection of UVR is discussed more comprehensively in the *SI Appendix*. We also explored the scenario where UVR does not change to serve as a lower bound. Each of these scenarios was used to drive photochemistry in the Title24 simulations in CMAQ. The Title24 SR changes as derived in the previous paragraph were used for the 410- to 850-nm wavelength band in the CMAQ simulations.

Emissions Processing. On-road NO_x and VOC along with biogenic VOC emissions profiles are dependent on meteorology. Annual hourly emissions profiles were developed as a function of the baseline and Title24 meteorological fields for the 2012 base year. The SoCAB emissions inventory is presented in ref. 1 and details of the emissions processing are presented in ref. 38. Changes in NO_x and VOC emissions in the baseline and Title24 simulations are small, mainly due to the similarity in the meteorological fields. Within the SoCAB, on average during the O₃ season, VOC emissions are reduced by 0.1% (0.75 tons per day) and NO_x emissions are reduced by $8 \times 10^{-4}\%$ (0.004 tons per day) in the Title24 scenario.

Within the SoCAB, changes in power-generation emissions are expected to be insignificant with the widespread implementation of cool roofs and are not accounted for in the modeling. Emissions from power generation are only responsible for 0.4% of the total NO_x emissions in the 2012 emission inventory. Additionally, only 37% of the total electricity consumed is generated within the SoCAB (1).

Meteorological and Chemical Transport Modeling. WRF version 3.6.1 was used with a North American Regional Reanalysis field to simulate 2012 meteorology on three nested grids, with an inner 4-km grid covering the modeling domain (*SI Appendix, Fig. S9*). (Details of the model setup are available in ref. 38.) WRF model performance is summarized in *SI Appendix, Figs. S10–*

S19. Two year-long simulations were performed: a base case using the MODIS-derived SR fields and a Title24 case using the modified SR fields detailed above assuming that all buildings in the SoCAB meet Title24 roof-top SR requirements.

CMAQ version 5.0.2 was used to simulate air quality without dynamic coupling within a 624- × 408-km modeling domain on a 4-km grid with 18 vertical layers. Extensive details of the modeling protocol are presented in ref. 38. Modification of the CMAQ code allowed us to calculate spatially resolved photolysis rate constants based on wavelength-dependent reflectance fields. As with any modeling study, results are dependent on the model accurately capturing the physical and chemical processes under investigation. *SI Appendix, Figs. S20–S28* summarize the ability of CMAQ to predict measured concentrations of O₃ and PM_{2.5} throughout the SoCAB.

Changes in annual averaged PM_{2.5}, daily maximum 8-h O₃, and daily maximum 1-h O₃ concentrations were evaluated across the modeling domain. Student's *t* tests for paired samples were conducted to determine whether changes in concentration across different scenarios were statistically significant. Differences with *P* values less than 0.05 were assumed to be statistically significant.

To evaluate the impact of widespread cool-roof installation toward attainment of federal ambient air-quality standards, relative response factor projections were also conducted to calculate changes in design values (DV). This strategy uses the ratio of Title24 vs. baseline concentrations to adjust measured values, cancelling out many of the systematic uncertainties responsible for concentration biases. This analysis is consistent with Environmental Protection Agency (EPA) modeling guidance (39) and is presented in ref. 38 with a summary in *SI Appendix*. Data and scripts, with minor exclusions (*SI Appendix*), are available with a South Coast Air Quality Management District public records request.

Results and Discussion

Changes in Meteorology. WRF simulations of 2012 meteorology representing the baseline (MODIS-derived SR) and Title24 (SR modified for cool-roof adoption) cases are summarized in Fig. 3. Annual averaged daily high temperatures are projected to decrease throughout the SoCAB (Fig. 3A) with the largest decreases (~0.35 K) in areas with the largest change in SR. Changes in the daily maximum planetary boundary layer height (PBLH) (Fig. 3B) are negative; the mixed layer height will decrease by 40–65 m in the most polluted areas of the SoCAB in the Title24 scenario, a significant difference compared with model-predicted average daily maximum mixed layer heights of 1–2 km. A decrease in surface temperature can reduce the buoyancy of the surface air, leading to a reduction in vertical mixing. Lower surface temperatures on land decrease the land–sea temperature gradient, slowing down the daytime sea breeze—an important mechanism that drives relatively clean marine air into the SoCAB. The average of the 9 AM-to-3 AM ventilation coefficient (VC), the integral of the horizontal wind velocity with respect to height at all layers below the maximum mixing depth (40) (Fig. 3C), decreases throughout the SoCAB with implementation of Title24. Daily profiles of the change in several meteorological variables are presented in *SI Appendix, Figs. S29–S32*.

Changes in PM_{2.5} Concentrations. Several year-long CMAQ simulations were conducted to determine the individual effects of changes in meteorology, emissions, enhanced SR, and a range of hypothetical changes in UVR. Fig. 4A shows the change in annual PM_{2.5} concentrations between the baseline simulation (scenario I in Table 2) and a simulation using Title24 meteorology, emissions resulting from the Title24 meteorology, and the assumption that UVR does not increase (scenario IV). Average PM_{2.5} concentrations increase throughout the SoCAB, presumably caused by reductions in mixing heights and VCs, as well as partitioning of semivolatile species to the particle phase at lower temperatures. In the populated central Los Angeles region and Long Beach, annual PM_{2.5} concentrations are projected to increase by approximately $0.3 \mu\text{g}\cdot\text{m}^{-3}$. Fig. 4B illustrates the change in the number of days that exceed the 24-h PM_{2.5} standard of $35 \mu\text{g}\cdot\text{m}^{-3}$ (scenario IV – scenario I). These changes

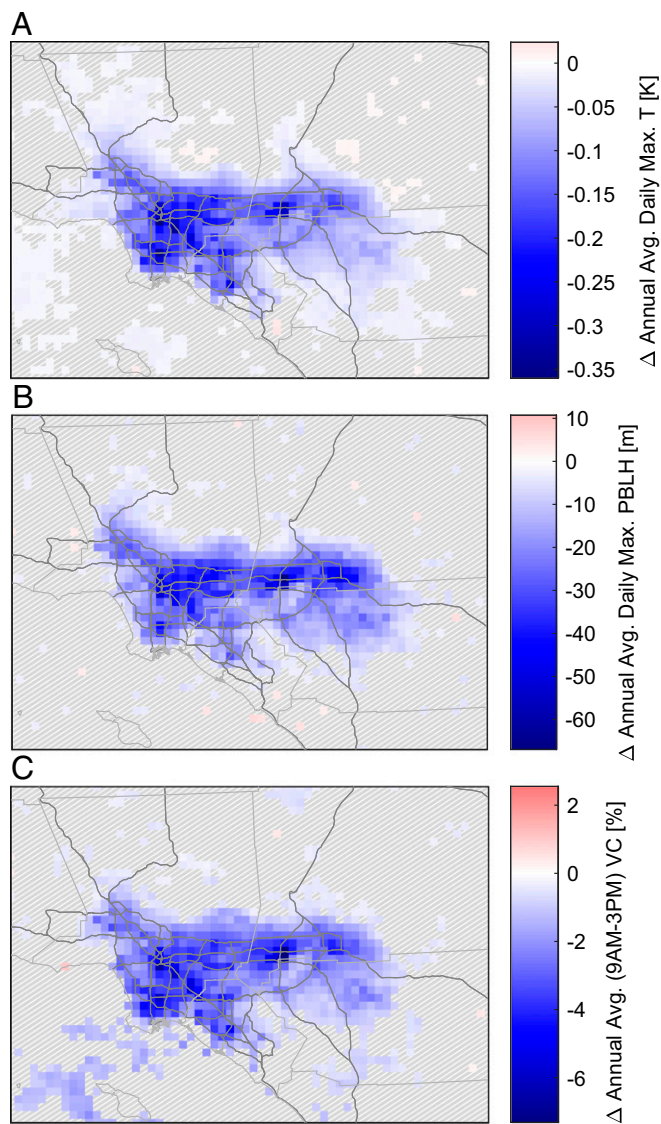


Fig. 3. (A) Change in annual average daily max temperatures (Title24 – baseline). (B) Change in annual average daily maximum PBLH. (C) Change in annual average VC calculated between 9 AM and 3 PM. Gray hashed cells indicate that differences are not statistically significant ($P > 0.05$).

are location-dependent, with increases in Los Angeles and the Inland Empire where $PM_{2.5}$ is typically highest.

Changes in annual averaged $PM_{2.5}$ at the Mira Loma monitoring location—the most polluted $PM_{2.5}$ station in the SoCAB—for each simulation are presented in Table 2. Implementation of Title24 emissions (scenario III) does not affect $PM_{2.5}$ concentrations relative to the baseline scenario (scenario I). However, the inclusion of Title24 meteorology (scenario IV) leads to an annual average $PM_{2.5}$ increase of $0.19 \pm 0.007 \mu\text{g}\cdot\text{m}^{-3}$. Increases in UVR (scenario V) lead to minimal changes in $PM_{2.5}$ concentrations.

Changes in SoCAB maximum annual and 24-h $PM_{2.5}$ policy-relevant DVs calculated with the EPA-recommended relative response factor approach are also shown in Table 2. SoCAB maximum annual DVs are expected to increase by approximately $0.2 \mu\text{g}\cdot\text{m}^{-3}$ even if increases in UVR are avoided—important compared with the $12 \mu\text{g}\cdot\text{m}^{-3}$ federal standards. Twenty-four-hour $PM_{2.5}$ DVs are projected to increase by $0.62\text{--}0.65 \mu\text{g}\cdot\text{m}^{-3}$

depending on changes in UVR—important compared with the 24-h $PM_{2.5}$ standard of $35 \mu\text{g}\cdot\text{m}^{-3}$.

Changes in Ozone Concentrations. Fig. 5 shows changes in daily maximum 8-h O_3 (DM8HO₃) concentrations averaged over the O_3 season (May 1–September 30) for two scenarios. Fig. 5A shows the changes expected if Title24 were fully implemented but UVR was held constant (scenario IV – scenario I). O_3 concentrations largely decrease throughout the SoCAB, with the exception of the Redlands area, which typically experiences the highest O_3 concentrations in the SoCAB. However, most residents in the SoCAB live in areas that will experience a decrease in O_3 under this scenario. Whereas the number of 75 ppb exceedance days is relatively unchanged in the most populated areas of the SoCAB, the number of exceedance days increase in the region surrounding Redlands (*SI Appendix, Fig. S35A*). Fig. 5B shows changes in O_3 concentrations resulting from an upper-bound change in UVR (scenario V – scenario I). Increases in average DM8HO₃ concentrations are expected in most of the SoCAB in this scenario (Fig. 5B). This translates to large increases in the number of exceedance days throughout the SoCAB (*SI Appendix, Fig. S35A*).

Table 2 details changes in mean \pm standard error (SE) DM8HO₃ concentrations at Redlands, the station with the highest 8-h O_3 DV. Changes in 1-h averaged daily maximum O_3 (DM1HO₃) concentrations are presented for Fontana, the monitoring station with the highest 1-h DVs in the SoCAB. Ozone concentrations are neither sensitive to increases in visible and IR reflectance (scenario II) within CMAQ nor to decreases in emissions inherent in the Title24 scenario (scenario III). Simulations with Title24 meteorology produce increases in averaged DM8HO₃ concentrations (scenarios IV and V). Depending on

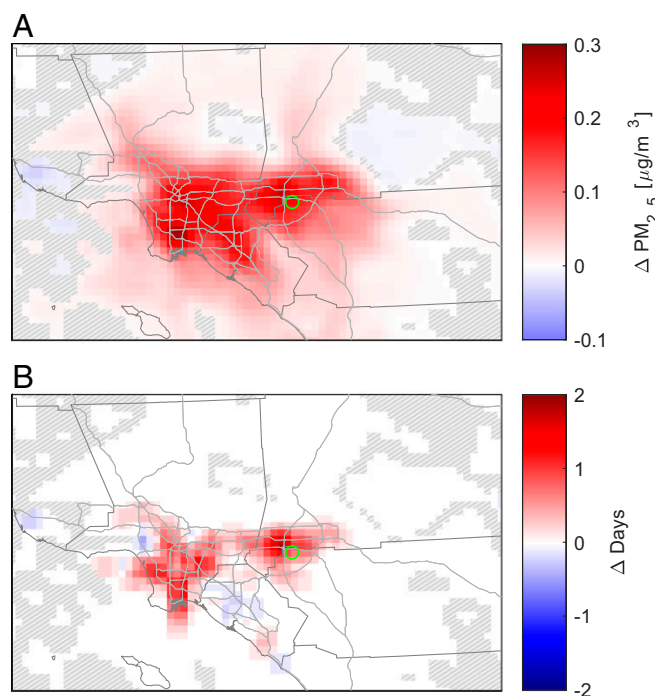


Fig. 4. (A) Change in annual average $PM_{2.5}$ concentrations (scenario IV – scenario I). The green circle indicates the location of the highest annual $PM_{2.5}$ measured DVs in the basin. Seasonal differences in $PM_{2.5}$ are presented in *SI Appendix, Fig. S34*. (B) Change in the number of 24-h $PM_{2.5}$ federal standard ($35 \mu\text{g}\cdot\text{m}^{-3}$) exceedance days in a year (scenario IV – scenario I). Gray hashed cells indicate that differences are not statistically significant ($P > 0.05$). Image represents 3×3 -cell moving average.

Table 2. Simulated changes in PM_{2.5} and O₃ at polluted locations

Scenario name	WRF SR	Emissions	Reflectance used to drive chemistry	Δ Annual average PM _{2.5} at Mira Loma, μg·m ⁻³	Δ Daily maximum 8-h O ₃ at Redlands, ppb	Δ Daily maximum 1-h O ₃ at Fontana, ppb	Δ Basin maximum annual PM _{2.5} DV, μg·m ⁻³	Δ Basin maximum 24-h PM _{2.5} DV, μg·m ⁻³	Δ Basin maximum 8-h O ₃ DV, ppb	Δ Basin maximum 1-h O ₃ DV, ppb
I	Baseline	Baseline	Baseline	0	0	0	0	0	0	0
II	Baseline	Baseline	Enhanced vis/IR, no UV increase	0.00 ± 0.000**	0.00 ± 0.000**	0.01 ± 0.000**	0	0	0	0
III	Baseline	Title24	Enhanced vis/IR, no UV increase	0.00 ± 0.000**	-0.01 ± 0.000**	-0.01 ± 0.001**	0	-0.07	0	0
IV	Title24	Title24	Enhanced vis/IR, no UV increase	0.19 ± 0.007**	0.04 ± 0.013**	-0.040 ± 0.023*	+0.23	+0.62	+0.3	-0.4
V	Title24	Title24	Enhanced vis/IR, maximum UV increase	0.20 ± 0.008**	0.66 ± 0.015**	0.96 ± 0.026**	+0.22	+0.65	+1.3	+1.9

Average concentrations are reported as nine cell averages (cell including station + eight adjacent cells). Uncertainty ranges represent the standard error. Δ indicates that the results of the baseline scenario were subtracted from the scenario indicated on each row. An additional scenario where UVR is increased to one-half of its maximum value is presented in *SI Appendix, Table S2*. **P* = 0.004; ***P* < 0.0001.

the magnitude of UVR increases, DM8HO₃ concentrations are projected to increase by 0.04 ± 0.013 (scenario IV) to 0.66 ± 0.015 ppb (scenario V), whereas DM1HO₃ concentrations are projected to change by -0.040 ± 0.023 to 0.96 ± 0.026 ppb. Although the increase in UVR in the upper-bound case is relatively small, ranging from 0 to 0.027 depending on location (Fig. 1B), ozone formation is still extremely sensitive to these increases. The projected changes in SoCAB-maximum DVs for 8-h and 1-h O₃ are presented in Table 2. Changes in O₃ concentrations and DVs are linearly dependent on the degree of UVR increases (*SI Appendix, Fig. S33 and Table S1*). The SoCAB maximum 8-h DV increases by 0.3 ppb with a constant UVR across the domain to 1.3 ppb with the UVR at the upper bound. Behavior of the 1-h SoCAB maximum DV is more complex. If increases in UVR can be avoided, the 1-h DV is expected to decrease by 0.4 ppb. However, if concentrations are simulated with maximum increases in UVR, 1-h O₃ DV concentrations can increase by 1.9 ppb. This counterintuitive behavior can be explained partially with Fig. 5. Fontana is further west than Redlands and is in the region where O₃ concentrations decrease when UVR is held constant and increase when UVR is at its maximum value. This illustrates the competition between the many factors governing O₃ concentrations that can change with cool-roof implementation.

Policy Implications. Attainment of the 75-ppb 8-h O₃ standard by 2031 in the SoCAB is an extremely challenging air-quality goal, requiring an additional 55% reduction in NO_x emissions beyond all existing regulations (1). Compliance with Title24 cool-roof standards may make attainment of this goal more difficult, even if future UVR increases are small. Scenario V assumes that buildings adopt cool roofing products with increase in UVR at an extreme upper bound. The actual increases in UVR throughout the SoCAB will depend on the individual roofing products that are chosen for installation. Although more realistic UVR increases cannot be projected without knowledge of the individual cool roofing products that are adopted, our analysis indicates that UVR will likely increase when replacing standard roofs with cool roofs. Whether ozone ultimately increases or decreases in the most populated areas of the basin will depend on the relative importance of multiple physicochemical pathways, including ozone decreases from temperature reductions, ozone increases from reduced ventilation and mixing, and ozone increases from possible UVR increases. Different magnitudes of SR increase or UVR increase may change the dominating mechanisms. We also simulated 2031 DVs with the presence of full Title24 implementation and full implementation of the proposed South Coast Air Quality

Management District control strategy (1). We estimate that even if UVR increases can be entirely avoided, Title24 could increase the 2031 8-h DV by 0.3 ppb and the 2031 1-h DV by 1.1 ppb. These increases in O₃ concentrations are consequential in light of the cost to reduce precursor emissions to achieve a corresponding reduction in O₃ concentrations.

Implementation of Title24 standards was used as the basis for this analysis; however, several factors may influence future adoption of cool roofs. Municipalities such as Los Angeles and Pasadena have cool-roof ordinances that can lead to increases in SR beyond what would be expected with the Title24 standards.

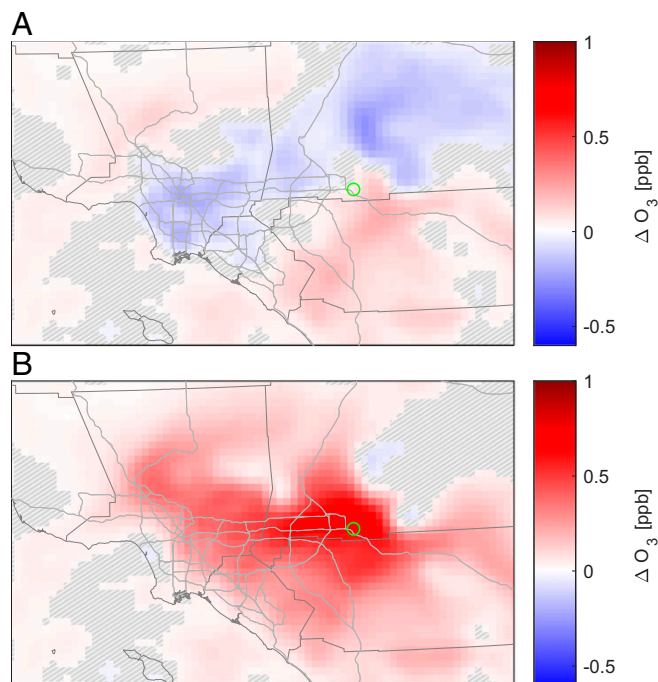


Fig. 5. (A) Change in annual average DM8HO₃ values (scenario IV) with the assumption that UVR does not change with widespread installation of cool roofs. The green circle indicates the location of the highest 8-h O₃ measured DVs in the basin. (B) Change in annual average DM8HO₃ values with the assumption that UVR increases are consistent with the maximum possible increase based on roofing products currently available (scenario V). Gray hashed cells indicate that differences are not statistically significant (*P* > 0.05). Image represents 3- × 3-cell moving average.

In addition, widespread adoption of solar photovoltaics and Title24 cool-roof installation exemptions for the implementation of equivalent energy savings measures could also affect future changes in urban reflectance.

The O₃ concentration sensitivity to small changes in cool-roof UVR supports the establishment of a standard regulating the UVR of certified cool-roof materials. Currently, materials must meet specific SR standards for consideration as a cool-roof material. Establishment of an additional UV standard could help minimize inadvertent increases in O₃. Furthermore, it is possible that a reduction in UVR below current values will lead to improvements in O₃ air quality throughout the SoCAB; this may be a cost-effective O₃ control strategy. Remote sensing measurements of the current rooftop stock to survey UVR could help set standards such that cool-roof materials do not lead to increases in UVR when they replace existing rooftops.

When assessing the impacts of cool roofs, it is important to consider all environmental and economic consequences. For example, benefits from a reduction in heat-related mortality may outweigh the increase in mortality from enhanced PM_{2.5} pollution. Also, widespread increases in urban SR can help to combat the local impacts of climate change. Potential energy bill savings are also an important benefit. In addition, there are other mechanisms

to control ambient air pollution such as emission reductions, whereas tools for mitigation of the urban heat island effect are more limited. Without a comprehensive analysis of all of the benefits of cool roofs it would be a mistake to discourage this technology solely on the basis of air quality alone.

Relatively small changes in surface reflectance lead to significant impacts in O₃ and PM_{2.5}. Results of this analysis also shed light on the choice of pavement materials and cool pavements, a potentially more important driver of overall urban SR and UVR. Analysis of impervious surface area (41) along with the rooftop area database developed for this paper indicates that there is significantly more pavement area in the SoCAB than rooftop area (1,900 km² of pavement area vs. 1,040 km² of rooftop area). (SI Appendix, Fig. S36 presents the spatial distribution of pavement area throughout the SoCAB.) In addition, only a fraction of the total rooftop area was modified for projections of air quality because Title24 does not affect rooftops in every climate zone. Therefore, the SR and UVR of pavements may be an important driver of regional air quality and human exposure to UV radiation and should be considered when evaluating cool pavement materials.

ACKNOWLEDGMENTS. This work was funded in part by NSF Grant CBET-1512429 (to G.B.-W.).

- South Coast Air Quality Management District (2016) Final 2016 air quality management plan (South Coast Air Quality Management District, Diamond Bar, CA).
- Akbari H, Pomerantz M, Taha H (2001) Cool surfaces and shade trees to reduce energy use and improve air quality in urban areas. *Sol Energy* 70:295–310.
- Vahmani P, Sun F, Hall A, Ban-Weiss G (2016) Investigating the climate impacts of urbanization and the potential for cool roofs to counter future climate change in Southern California. *Environ Res Lett* 11:124027.
- Zhang J, Zhang K, Liu J, Ban-Weiss G (2016) Revisiting the climate impacts of cool roofs around the globe using an Earth system model. *Environ Res Lett* 11:084014.
- Stone B, Jr, et al. (2014) Avoided heat-related mortality through climate adaptation strategies in three US cities. *PLoS One* 9:e100852.
- Georgescu M, Morefield PE, Bierwagen BG, Weaver CP (2014) Urban adaptation can roll back warming of emerging megapolitan regions. *Proc Natl Acad Sci USA* 111: 2909–2914.
- Santamouris M (2014) Cooling the cities: A review of reflective and green roof mitigation technologies to fight heat island and improve comfort in urban environments. *Sol Energy* 103:682–703.
- Ban-Weiss GA, Woods J, Levinson R (2015) Using remote sensing to quantify albedo of roofs in seven California cities, part 1: Methods. *Sol Energy* 115:777–790.
- Ban-Weiss GA, Woods J, Millstein D, Levinson R (2015) Using remote sensing to quantify albedo of roofs in seven California cities, part 2: Results and application to climate modeling. *Sol Energy* 115:791–805.
- Li D, Bou-Zeid E, Oppenheimer M (2014) The effectiveness of cool and green roofs as urban heat island mitigation strategies. *Environ Res Lett* 9:055002.
- Doulos L, Santamouris M, Livada I (2004) Passive cooling of outdoor urban spaces. The role of materials. *Sol Energy* 77:231–249.
- Santamouris M, Synnefa A, Karlessi T (2011) Using advanced cool materials in the urban built environment to mitigate heat islands and improve thermal comfort conditions. *Sol Energy* 85:3085–3102.
- Li D, Bou-Zeid E (2013) Synergistic interactions between urban heat islands and heat waves: The impact in cities is larger than the sum of its parts. *J Appl Meteorol Climatol* 52:2051–2064.
- Millstein D, Menon S (2011) Regional climate consequences of large-scale cool roof and photovoltaic array deployment. *Environ Res Lett* 6:034001.
- Akbari H, Levinson R (2008) Evolution of cool-roof standards in the US. *Adv Build Energy Res* 2:1–32.
- Levinson R, Akbari H (2009) Potential benefits of cool roofs on commercial buildings: Conserving energy, saving money, and reducing emission of greenhouse gases and air pollutants. *Energy Effic* 3:53–109.
- Menon S, Akbari H, Mahanama S, Sednev I, Levinson R (2010) Radiative forcing and temperature response to changes in urban albedos and associated CO₂ offsets. *Environ Res Lett* 5:014005.
- Akbari H, Menon S, Rosenfeld A (2009) Global cooling: Increasing world-wide urban albedos to offset CO₂. *Clim Change* 94:275–286.
- Akbari H, Matthews HD, Seto D (2012) The long-term effect of increasing the albedo of urban areas. *Environ Res Lett* 7:024004.
- Jacobson MZ, Ten Hoeve JE (2011) Effects of urban surfaces and white roofs on global and regional climate. *J Clim* 25:1028–1044.
- Sharma A, et al. (2016) Green and cool roofs to mitigate urban heat island effects in the Chicago metropolitan area: Evaluation with a regional climate model. *Environ Res Lett* 11:064004.
- Taha H (2008) Meso-urban meteorological and photochemical modeling of heat island mitigation. *Atmos Environ* 42:8795–8809.
- Taha H (2015) Meteorological, air-quality, and emission-equivalence impacts of urban heat island control in California. *Sustainable Cities and Soc* 19:207–221.
- Taha H (2009) Urban surface modification as a potential ozone air-quality improvement strategy in California—Phase Two: Fine-resolution meteorological and photochemical modeling of urban heat islands (Altostratus Inc., Martinez, CA), Report CEC-500-2009-071.
- Taha H (2008) Urban surface modification as a potential ozone air-quality improvement strategy in California: A mesoscale modelling study. *Boundary Layer Meteorol* 127:219–239.
- Taha H (1997) Modeling the impacts of large-scale albedo changes on ozone air quality in the South Coast Air Basin. *Atmos Environ* 31:1667–1676.
- Taha H (2005) Urban surface modification as a potential ozone air-quality improvement strategy in California—Phase One: Initial mesoscale modeling (Altostratus Inc., Martinez, CA), Report CEC-500-2005-128.
- Edwards PM, et al. (2014) High winter ozone pollution from carbonyl photolysis in an oil and gas basin. *Nature* 514:351–354.
- Fallmann J, Forkel R, Emeis S (2016) Secondary effects of urban heat island mitigation measures on air quality. *Atmos Environ* 125:199–211.
- California Energy Commission (2012) Building energy efficiency standards for residential and nonresidential buildings. Title 24 Part 6 and associated administrative regulations in Part 1 (California Energy Commission, Sacramento, CA).
- South Coast Air Quality Management District (2016) Final socioeconomic report 2016 air quality management plan (South Coast Air Quality Management District, Diamond Bar, CA).
- Building Vectors, ed, Geospatial Repository and Data Management System (GRiD) Cold Regions Research and Engineering Laboratory (CRREL) Engineer Research and Development Center (ERDC) (US Army Corps of Engineers, Washington, DC).
- Vahmani P, Ban-Weiss GA (2016) Impact of remotely sensed albedo and vegetation fraction on simulation of urban climate in WRF-urban canopy model: A case study of the urban heat island in Los Angeles. *J Geophys Res Atmos* 121:1511–1531.
- Finlayson-Pitts BJ, Pitts JN, Jr (2000) *Chemistry of the Upper and Lower Atmosphere* (Academic, San Diego).
- Parker DS, McIlvaine JER, Barkaszi SF, Beal DJ, Anello MT (2000) Laboratory testing of the reflectance properties of roofing material (Florida Solar Energy Center, Cocoa, FL).
- Prado RTA, Ferreira FL (2005) Measurement of albedo and analysis of its influence the surface temperature of building roof materials. *Energy Build* 37:295–300.
- Berdahl P, Bretz SE (1997) Preliminary survey of the solar reflectance of cool roofing materials. *Energy Build* 25:149–158.
- South Coast Air Quality Management District (2016) Final 2016 air quality management plan appendix V: Modeling and attainment demonstrations (South Coast Air Quality Management District, Diamond Bar, CA).
- US Environmental Protection Agency (2014) Draft modeling guidance for demonstrating attainment of air quality goals for ozone, PM_{2.5}, and regional haze (US Environmental Protection Agency, Washington, DC).
- Ashrafi K, Shafie-Pour M, Kamalan H (2009) Estimating temporal and seasonal variation of ventilation coefficients. *Int J Environ Res* 3:637–644.
- Xian G, et al. (2011) Change of impervious surface area between 2001 and 2006 in the conterminous United States. *Photogramm Eng Remote Sensing* 77:758–762.

Supporting Information Appendix

Air Quality Implications of Widespread Adoption of Cool Roofs on Ozone and Particulate Matter in Southern California

Scott A. Epstein¹, Sang-Mi Lee¹, Aaron S. Katzenstein¹, Marc Carreras-Sospedra¹, Xinqiu Zhang¹, Salvatore Farina¹, Pouya Vahmani², Philip M. Fine¹, and George Ban-Weiss²

¹South Coast Air Quality Management District

Planning, Rules, and Area Sources Division

21865 Copley Drive

Diamond Bar, CA 91765-4178

²Sonny Astani Department of Civil and Environmental Engineering

University of Southern California

3620 S. Vermont Avenue, KAP 210

Los Angeles, CA 90089-2531

Corresponding Author: Scott A. Epstein, 21865 Copley Drive, Diamond Bar CA 91765-4178,
sepstein@aqmd.gov

SI Materials and Methods

Development of Building Footprint Database

With Southern California Association of Governments (SCAG) land use categories(1) and US Army Corps of Engineers building footprint data (containing rooftop perimeters and average rooftop slope), it was possible to determine the area of buildings in each of the six Title24 categories in each grid cell. However, interpolation was necessary to determine the rooftop area in grid cells without building footprint data (Figure S2). Building area was not interpolated directly. Instead, we interpolated two somewhat smoothly varying parameters: the plan area fraction and the fraction of low slope buildings. While the interpolation introduces some uncertainty, the majority of rooftop area in the SoCAB is explicitly defined in the datasets and does not come from interpolated parameters.

First, SCAG land use categories were translated to Title24 categories. The parcel area in each category was determined in each grid cell (Figure S3) without regard for building slope. The area of buildings lying within each of these three Title24 land use categories could then be tallied (Figure S4). However, since the US Army Corps of Engineers data does not cover the entire SoCAB, we were only able to initially calculate building area for the regions covered by the dataset. Next, we calculated the plan area fraction—defined as the area occupied by buildings normalized by the entire parcel area in each of the three Title24 land use categories (Figure S5 upper panes). Since the plan area fraction is somewhat of a smooth function throughout the Basin, it was reasonable to interpolate this field using a natural neighbor interpolation scheme to calculate the plan area fraction in grid cells without building footprint data (Figure S5 lower panes). Cells with actual data were not replaced by the interpolated fields. The building footprint data was then processed such that each building was tagged as either low-slope or high-slope. This data could then be integrated with the land use data to determine the low-slope fraction (area of low slope rooftops / total building area) in each of the three Title24 land use categories (Figure S6 upper panes). This low-slope fraction was then interpolated to fill in the missing grid cells (Figure S6 lower panes). As in the plan area fraction interpolation, cells with actual data were not replaced by the interpolated fields. The plan area fraction fields, the low-slope fraction fields, and the land use fields could then be combined to determine the rooftop area in each of the six Title24 categories throughout the entire Basin (Figure S7).

Projection of UVR for CMAQ Modeling

Unlike solar reflectance (SR), UV reflectance (UVR) measurements of the current building stock are not available. Therefore, we designed a method to project future UVR to represent an extreme upper-bound case. The methodology implemented for the analysis is detailed in the

main manuscript and shown as a schematic in Figure S8. However, there are other methods to estimate future UVR under an extreme upper-bound case. Fortunately, our conclusions are not highly sensitive to exactly where this upper-bound is established. The upper-bound CMAQ simulations should not be interpreted as a likely future scenario; the results of these simulations establish that between the lower-bound UVR projection case (UVR remains unchanged in the future) and the upper-bound UVR projection case, ozone concentrations are sensitive to changes in UVR and increase as UVR increases. The overall sensitivity of ozone concentrations to UVR changes is linear in the region of the SoCAB with the highest ozone concentrations (Figure S33) and can be used to estimate ozone with more realistic changes in UVR.

We explored another extreme upper-bound UVR projection methodology to test the sensitivity of our UVR projection. In this methodology, roofing materials with reflectance measurements are grouped in the same fashion as detailed in the main document to represent high-slope cool materials, high-slope standard materials, low-slope cool materials, and low-slope standard materials. For each roofing material, the ratio of reflectance within a specific wavelength range is normalized by the visible reflectance of that material (UVR/SR). A single high-UVR material is selected to represent the high-slope cool materials by identifying the product that has the highest normalized reflectance ratio (UVR/SR) in the first five UV wavelength bands (290nm-300nm, 300nm-310nm, 310nm-315nm, 315nm-320nm, and 320nm-345nm). A single low-UVR material is selected to represent the low-slope standard materials by identifying the product that has the lowest normalized reflectance ratio in the first five UV wavelength bands. In the same fashion, a single high-UVR material and a single low-UVR material were selected to represent low-slope cool materials and low-slope standard materials, respectively. In order to calculate the base-case UVR at each wavelength range, the reflectance ratios of the two identified low-slope and high-slope standard products were multiplied by the current SR in each land-use category from remote sensing measurements (See Table 1). In the same fashion, the reflectance ratios of the two cool products were multiplied by the corresponding Title24 projected SR to estimate the upper-bound Title24 UVR at each wavelength range for each land-use category. Upper-bound projected wavelength-dependent changes in reflectance for rooftops in each land-use category could then be calculated by subtracting the corresponding cool UVR from the corresponding standard UVR. The analogous values were calculated for the high-slope materials. These upper-bound projected changes in wavelength dependent UVR could then be weighted by the fraction of each Title24 land-use category in each grid-cell as performed for the methodology detailed in the manuscript. This strategy produces upper-bound UVR values that are slightly higher than the upper-bound UVR values calculated with the original methodology in the first four wavelength bands where photons have the most energy to induce photochemistry. Upper-bound UVR values calculated from this methodology are slightly lower than the upper-bound UVR values calculated with the original methodology in the two lower energy UV wavelength bands.

Calculation of Design Values and Relative Response Factor Based Projections

Design values are used to determine attainment of the National Ambient Air Quality Standards as outlined in the United States Clean Air Act. 8-hour ozone, 1-hour ozone, 24-hour average PM_{2.5} and annual average PM_{2.5} design values were calculated. 8-hour ozone design values are based on the fourth highest daily maximum eight-hour averaged concentration throughout the ozone season. These 8-hour values are averaged over a three year period. 1-hour ozone design values are based on the fourth highest one-hour daily maximum ozone concentration in a three year period. Annual average PM_{2.5} design values are based on the average of all the daily PM_{2.5} concentrations while 24-hour averaged PM_{2.5} design values are based on the 98th percentile highest-concentration day in a year. In order to minimize the effects of year-to-year variations in meteorology and/or emissions, three adjacent three-year design values are then averaged to generate five-year weighted design values. Moreover, design values for 2012, the base-year of our simulations, incorporates measurement data from 2010 to 2014 with the most weight assigned to 2012 and the least weight assigned to 2010 and 2014. To evaluate changes in policy-relevant design values, a relative response factor (RRF) approach is used to project baseline 2012 5-year weighted design values (2, 3). RRFs capture the ratio of Title24 and baseline concentrations. The 8-hour ozone RRFs are based on the ratio of daily-maximum concentrations on the days with the top 10 highest concentrations in the baseline simulations. The 1-hour ozone RRFs use the ratio of daily -maximum concentrations on the days with the top three highest concentrations in the baseline simulations. Design values for the "Title24" simulations are the product of the baseline design values and the RRFs at each measurement location. The annual RRFs are species specific (nitrate, sulfate, organic carbon, elemental carbon, crustal material, salt, and ammonium) and are based on the average of quarterly averaged concentrations in the baseline and Title24 simulations. These species specific RRFs are then applied to the specific design values at each measurement location. Annual PM_{2.5} design values for the "Title24" simulations are the sum of the product of each species' baseline design value and RRF.

Data Sharing

All data used in the paper is available publicly via a South Coast Air Quality Management District public records request with the following restrictions:

- Raw building footprint data used to build the database of buildings in the South Coast Air Basin were acquired from the US Army Corps of Engineers. We are unable to share this data as it is labeled "for official use only." The processed product used for the meteorological and air quality modeling is available.
- Roof manufacturer and model names for products measured and reported in Figure 2 cannot be shared with the public, but the spectral reflectance data is available.

References

1. 2012 Regional Transportation Plan/Sustainable Communities Strategy. (Southern California Association of Governments, Los Angeles, CA).
2. Final 2016 Air Quality Management Plan Appendix V: Modeling and Attainment Demonstrations. (South Coast Air Quality Management District, Diamond Bar, CA).
3. U.S. Environmental Protection Agency (2014) Draft Modeling Guidance for Demonstrating Attainment of Air Quality Goals for Ozone, PM_{2.5}, and Regional Haze.

Supporting Information Tables

Table S1: Simulated changes in PM_{2.5} and O₃ at polluted locations to illustrate how air quality responds to incremental changes in surface UV albedo

WRF albedo	Emissions	Albedo Used to Drive Chemistry	Δ Annual Average PM _{2.5} at Mira Loma (μg m ⁻³)	Δ Daily-Maximum 8-Hour O ₃ at Redlands (ppb)	Δ Daily Maximum 1-Hour O ₃ at Fontana (ppb)	Δ Basin Max. Ann. PM _{2.5} DV (μg m ⁻³)	Δ Basin Max. 24-Hr PM _{2.5} DV (μg m ⁻³)	Δ Basin Max. 8-Hr O ₃ DV (ppb)	Δ Basin Max. 1-Hr O ₃ DV (ppb)
Title24	Title24	Enhanced Vis/IR, no UV increase	0.19 ± 0.007 p<0.0001	0.04 ± 0.013 p<0.0001	-0.040 ± 0.023 p=0.004	+0.23	+0.62	+0.3	-0.4
Title24	Title24	Enhanced Vis/IR ½ Max UV increase	0.19 ± 0.007 p<0.0001	0.35±0.013 p<0.0001	0.46 ± 0.024 p<0.0001	+0.20	+0.60	+0.8	+0.7
Title24	Title24	Enhanced Vis/IR Max UV increase	0.20 ± 0.008 p<0.0001	0.66 ± 0.015 p<0.0001	0.96 ± 0.026 p<0.0001	+0.22	+0.65	+1.3	+1.9

Table S2: Roof types used to represent low slope and high slope roofing materials

Low slope	High slope
Asphalt shingle	Modified bitumen Single-ply membrane Field applied coating Factory applied coating

Supporting Information Figures

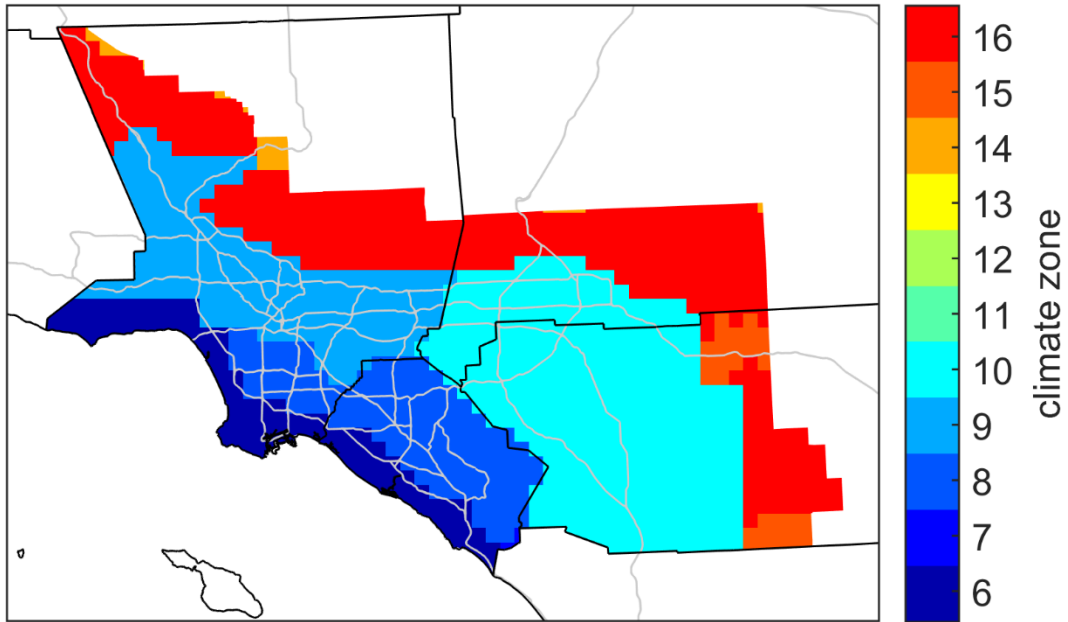


Figure S1: Gridded climate zone map of the South Coast Air Basin. Climate zone numbers are established by the California Energy Commission.

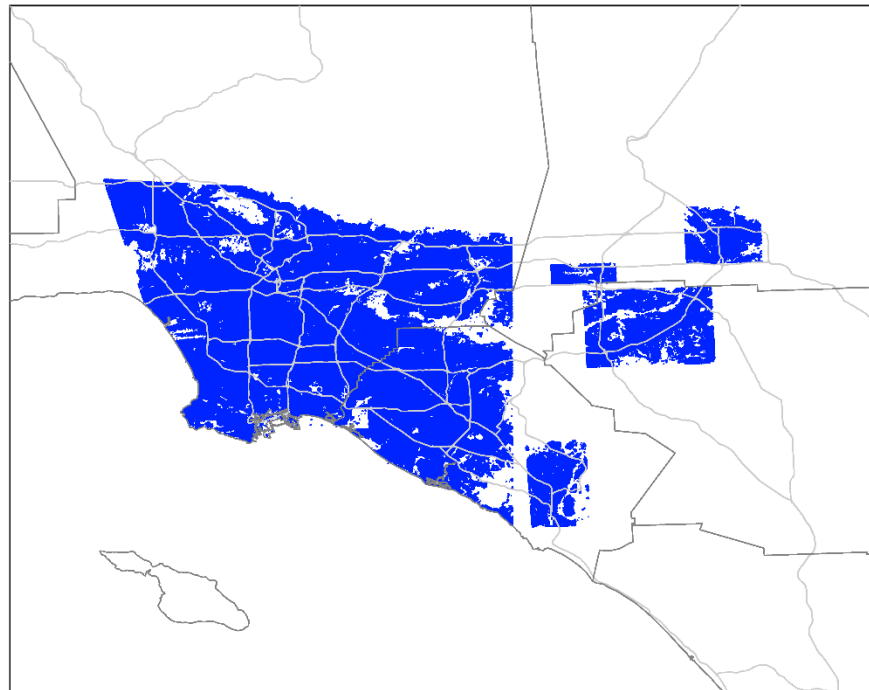


Figure S2: Area of the Basin with available building footprint data

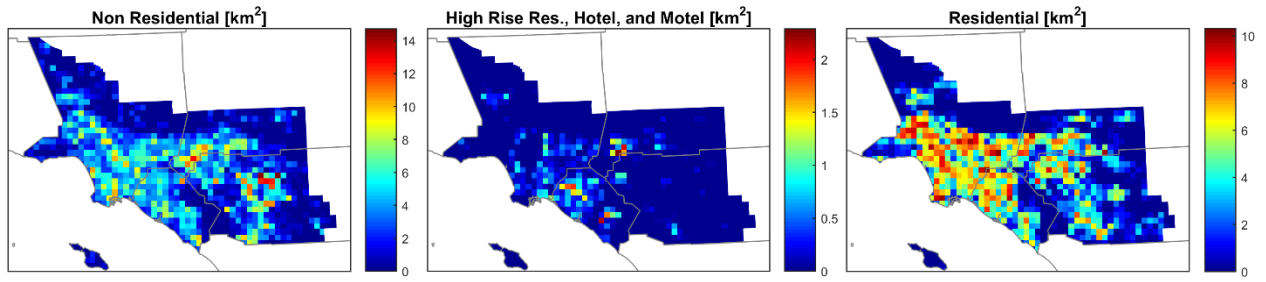


Figure S3: Land use area in each grid cell for the Title24 categories from the SCAG dataset

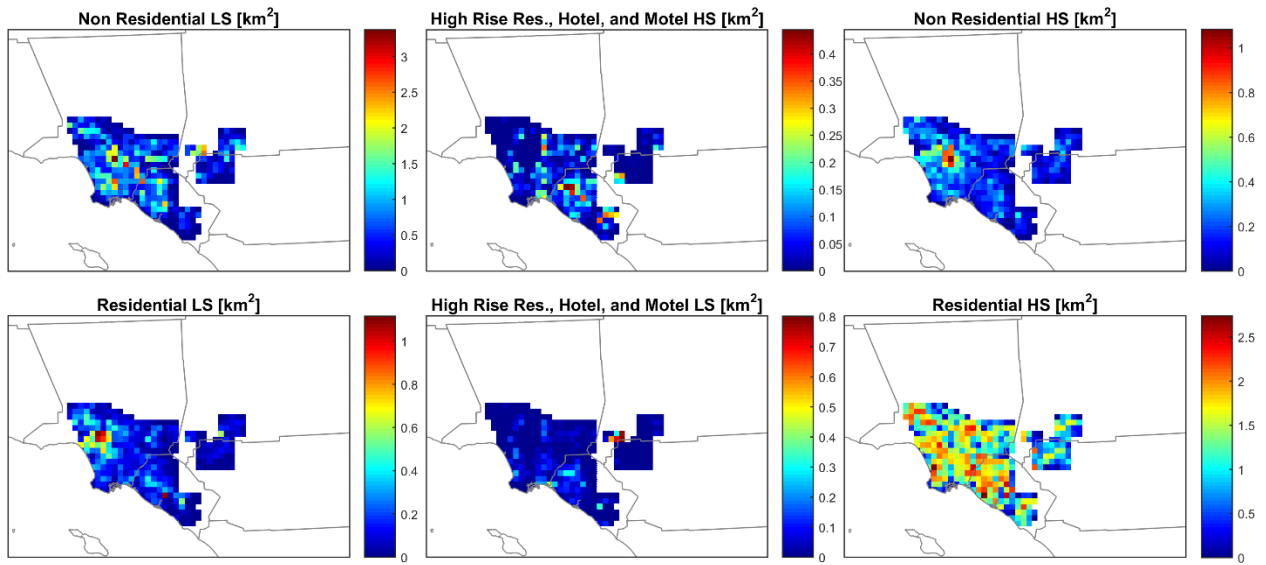


Figure S4: Building area in each grid cell for the Title24 categories calculated from the US Army Corps of Engineers dataset and the SCAG dataset

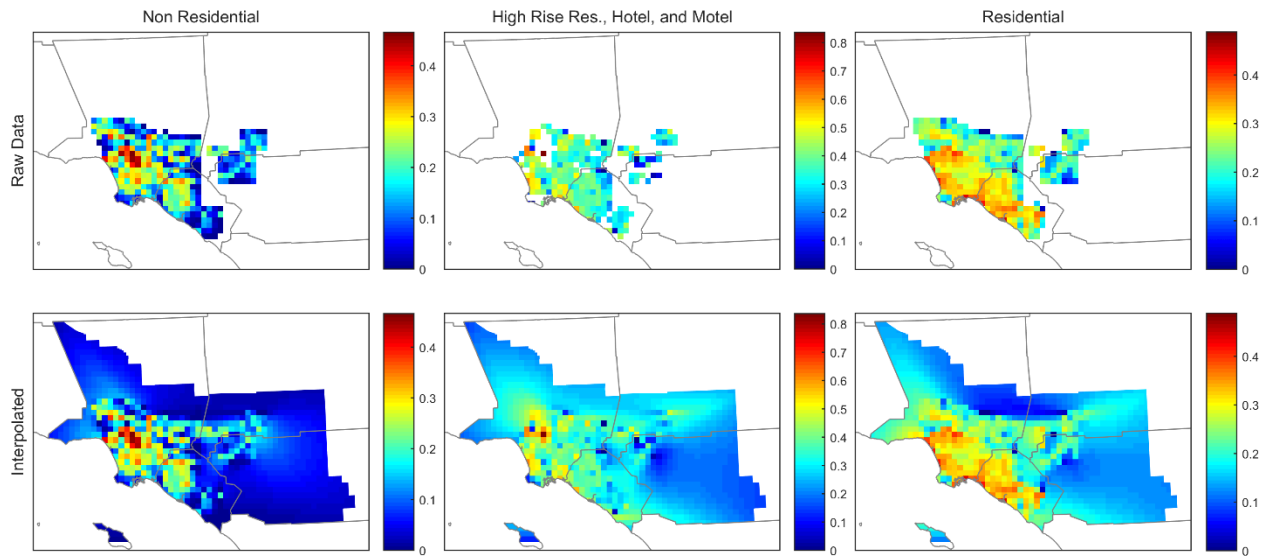


Figure S5: Plan area fraction for the Title24 categories (building area / plan area). This fraction is calculated from the US Army Corps of Engineers dataset and the SCAG dataset. The data in bottom row are interpolated from the data in the top row.

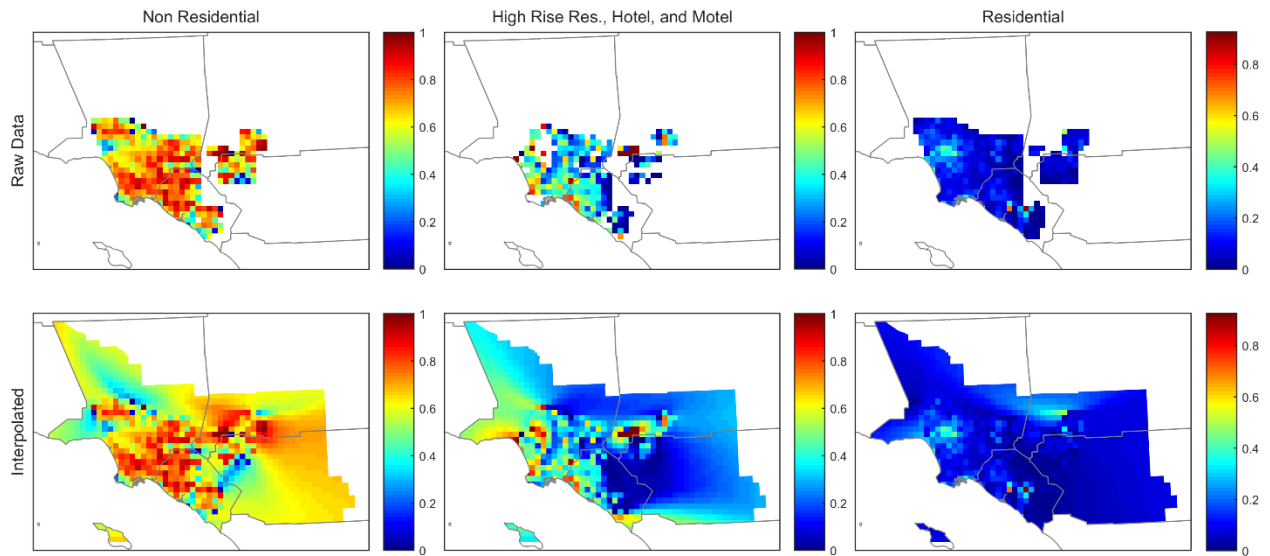


Figure S6: Fraction of building area that has low-slope rooftops. This fraction is calculated from the US Army Corps of Engineers dataset and the SCAG dataset. The data in bottom row are interpolated from the data in the top row.

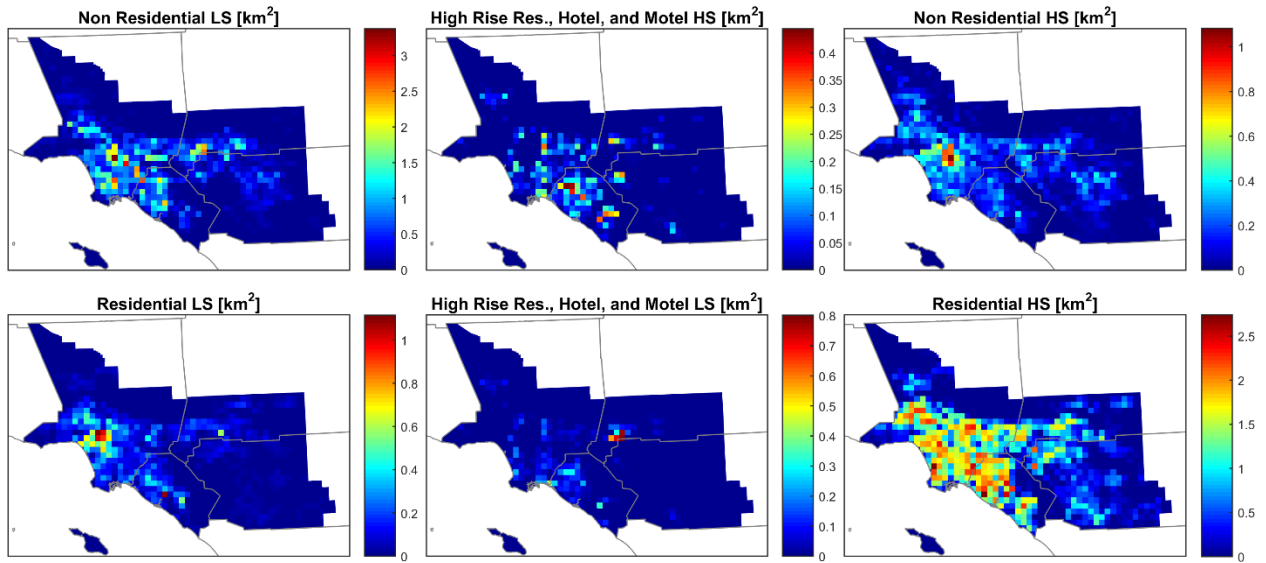
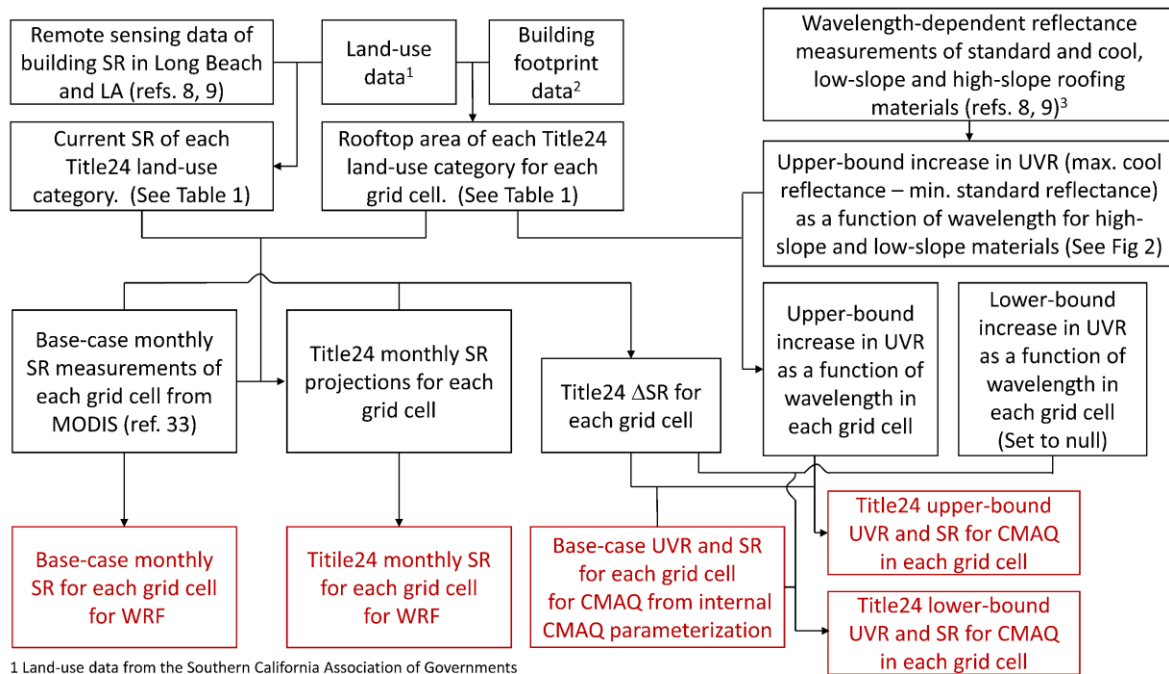


Figure S7: Calculated building area in each of the six Title24 categories.



1 Land-use data from the Southern California Association of Governments
 2 Building footprint data from the US Army Corps of Engineers (ref. 32)
 3 Reflectance measurements were not available between 290 and 300 nm. Reflectance measurements from 300-310 were used to estimate reflectance in this wavelength range

Figure S8: Schematic representation of the procedure used to project SR and UVR for WRF and CMAQ simulations. Red boxes are the final products of the analysis.



Figure S9: Extent of the CMAQ modeling domain

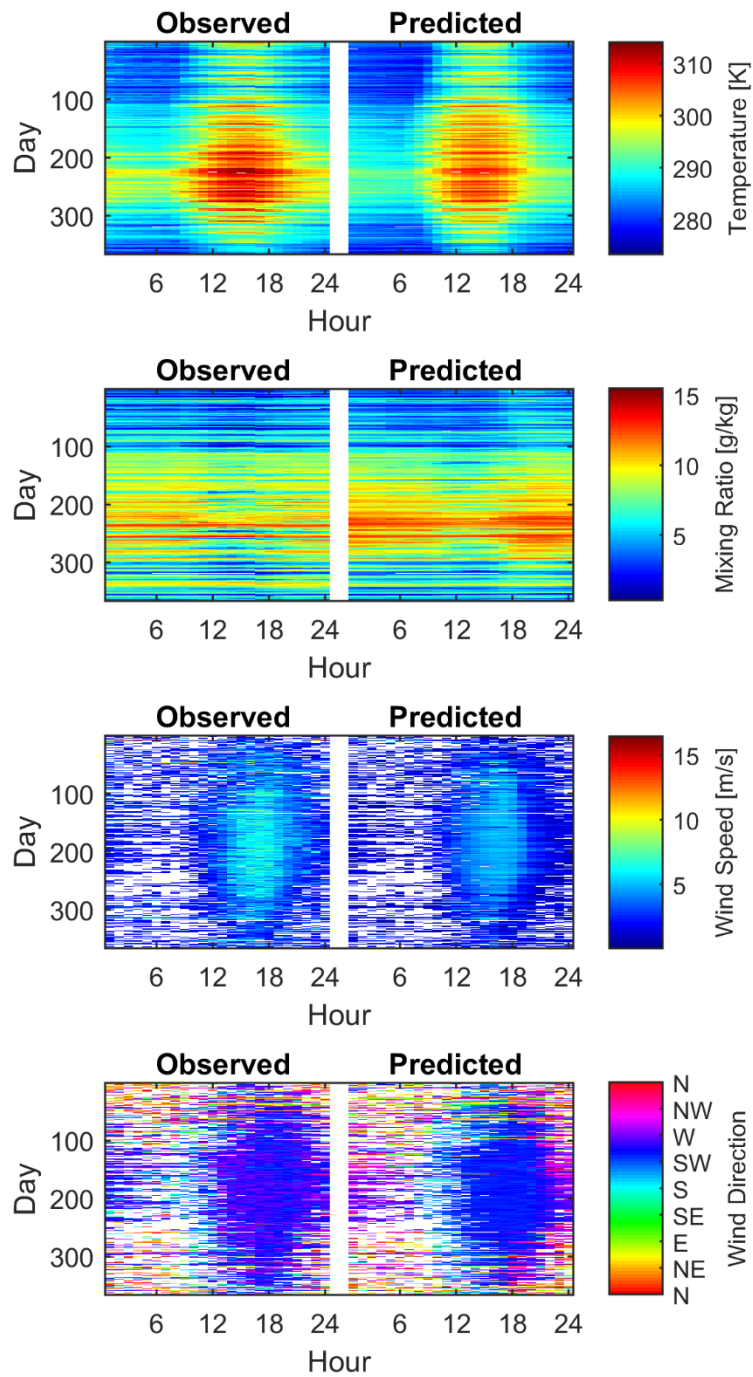


Figure S10: Comparison of measurements and model-predicted meteorological parameters for 2012 at LA/Ontario International Airport in Ontario, California.

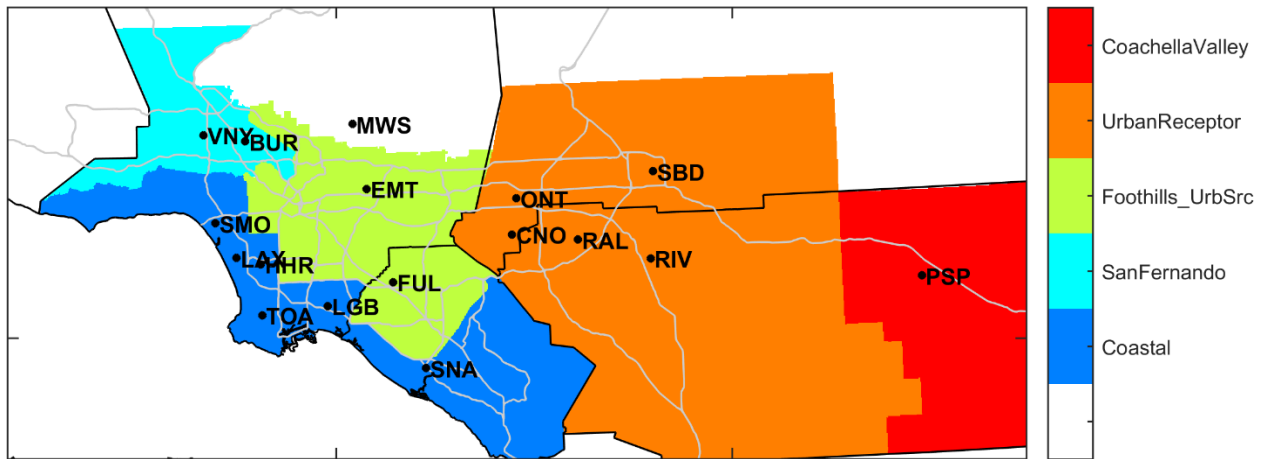


Figure S11: WRF model-performance regions and National Climatic Data Center meteorological stations (black circles) that we used for the model/measurement comparisons

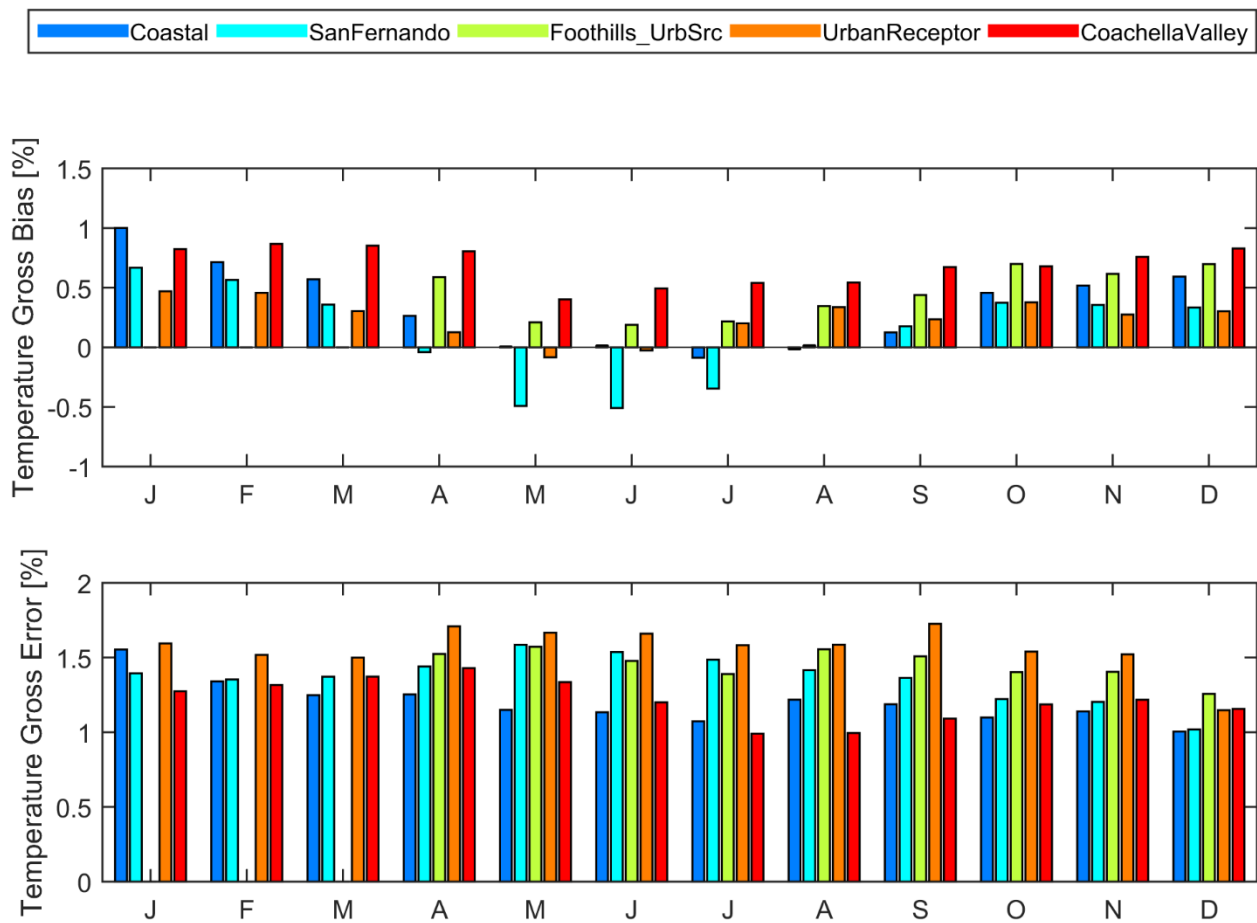


Figure S12: WRF model performance for predictions of 2m temperature in each WRF model-performance region for each month of the year

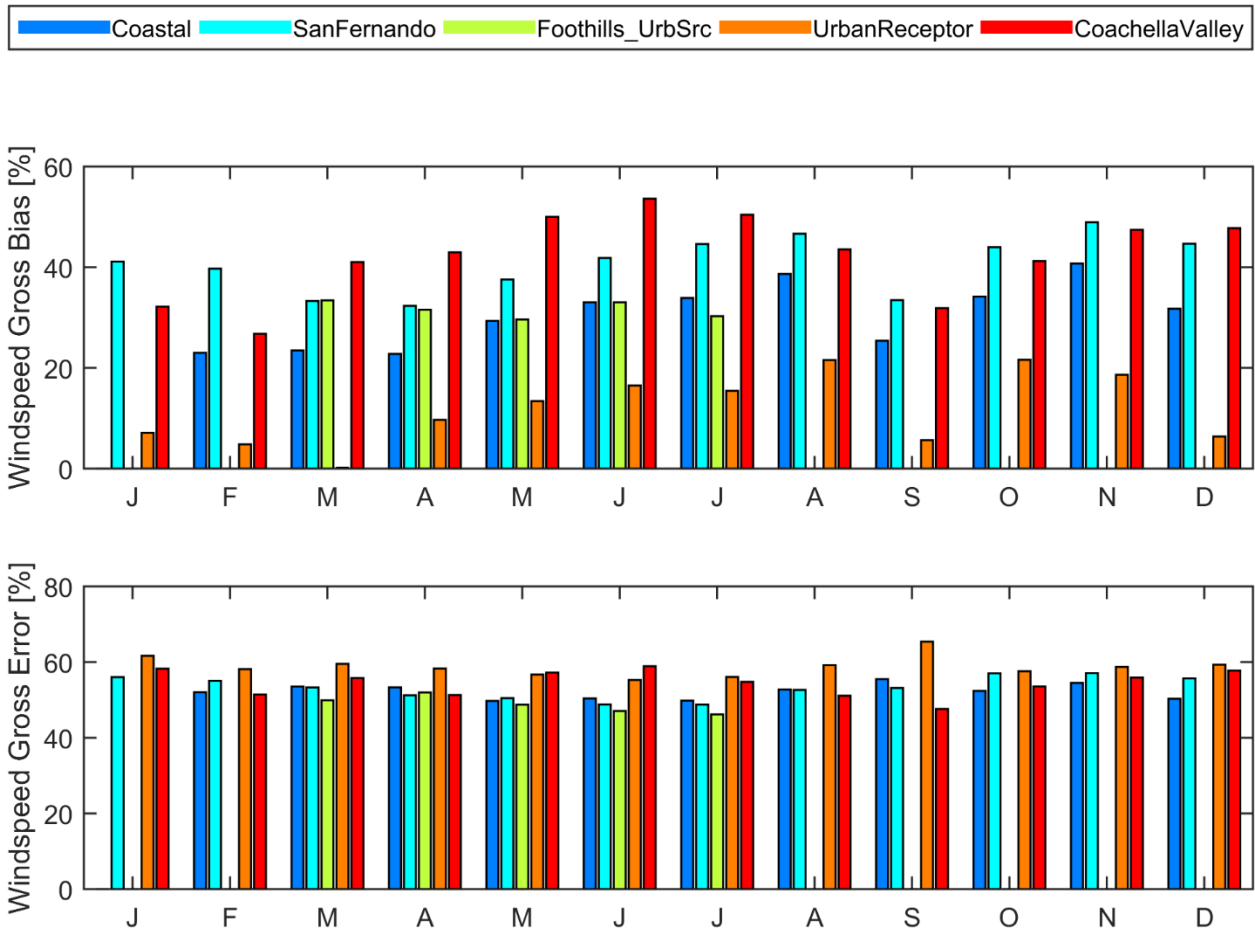


Figure S13: WRF model performance for predictions of surface wind speed in each WRF model-performance region for each month of the year

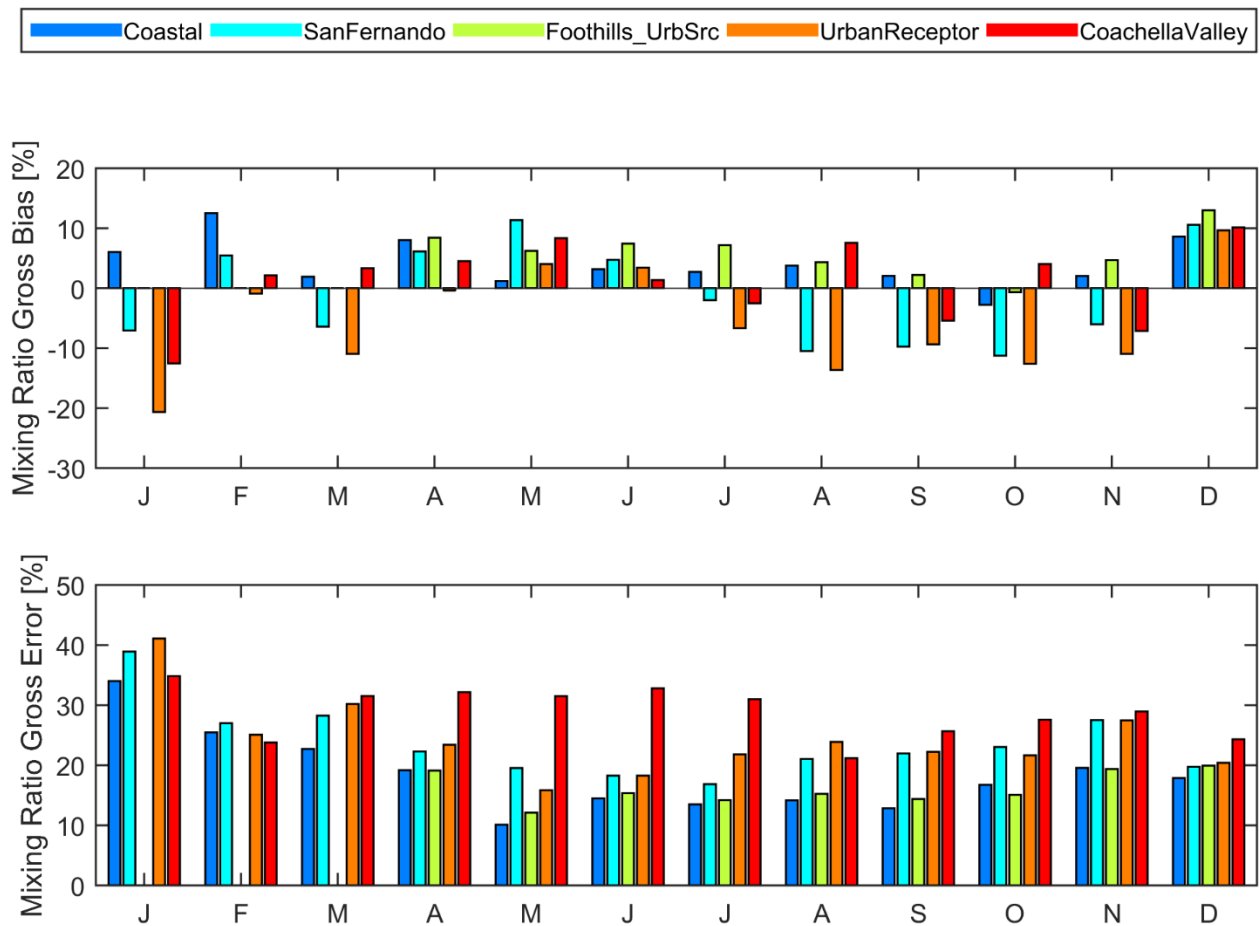


Figure S14: WRF model performance for predictions of water mixing ratio in each WRF model-performance region for each month of the year

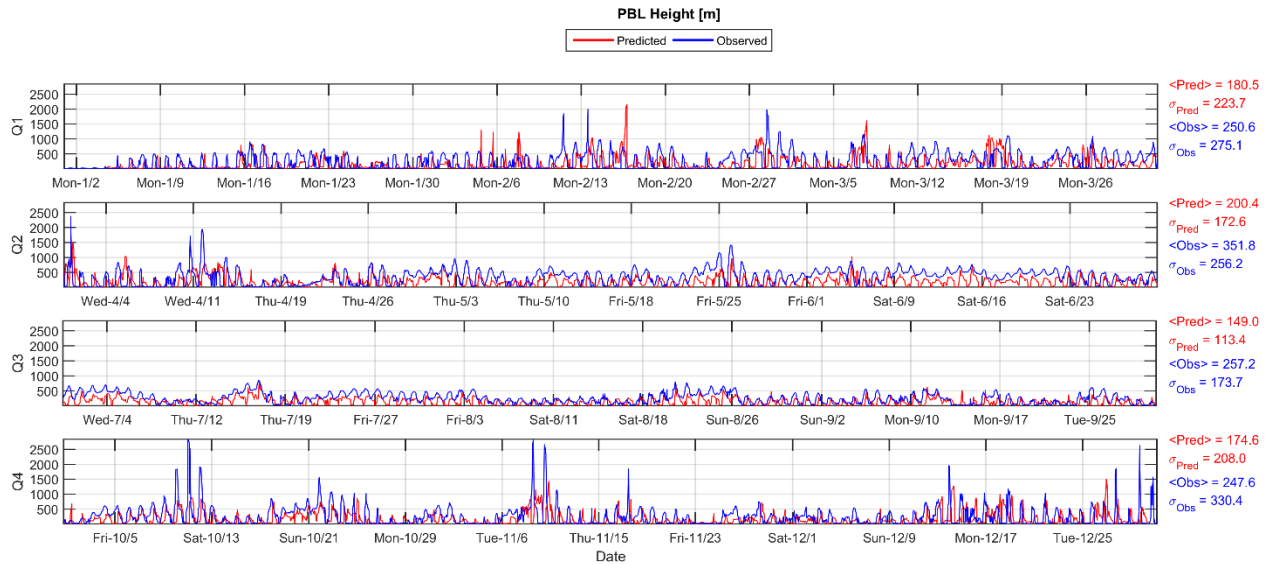


Figure S15: Planetary boundary layer height model performance at Los Angeles International Airport. PBL height estimates were calculated from continuous radiometer measurements (2).

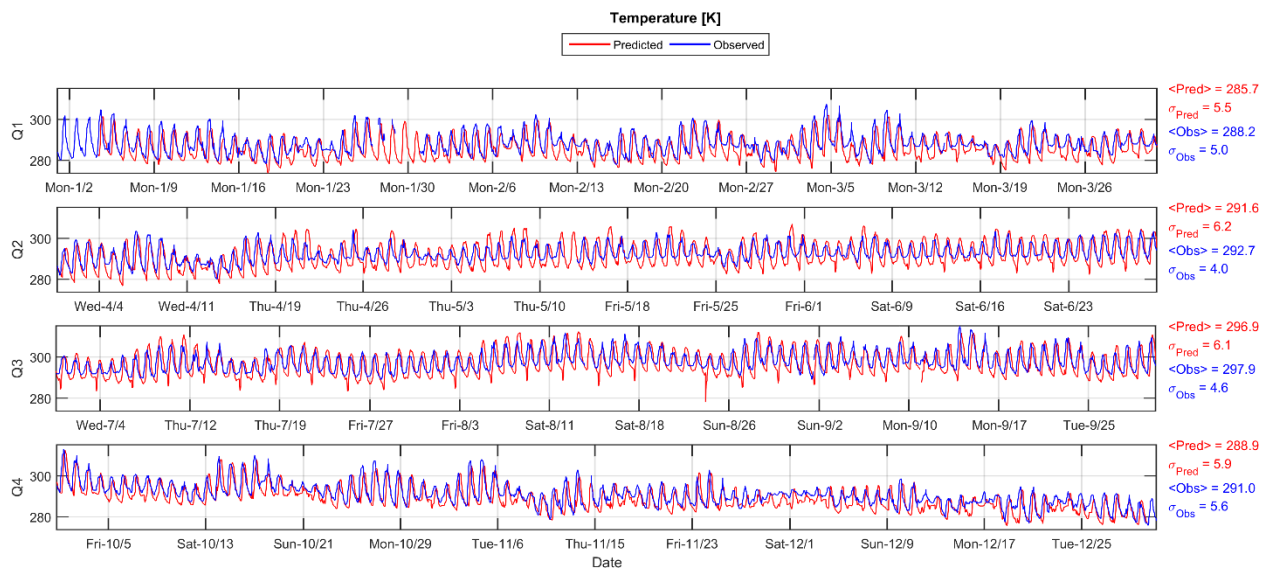


Figure S16: Yearly time series of temperature observations and predictions in Fullerton

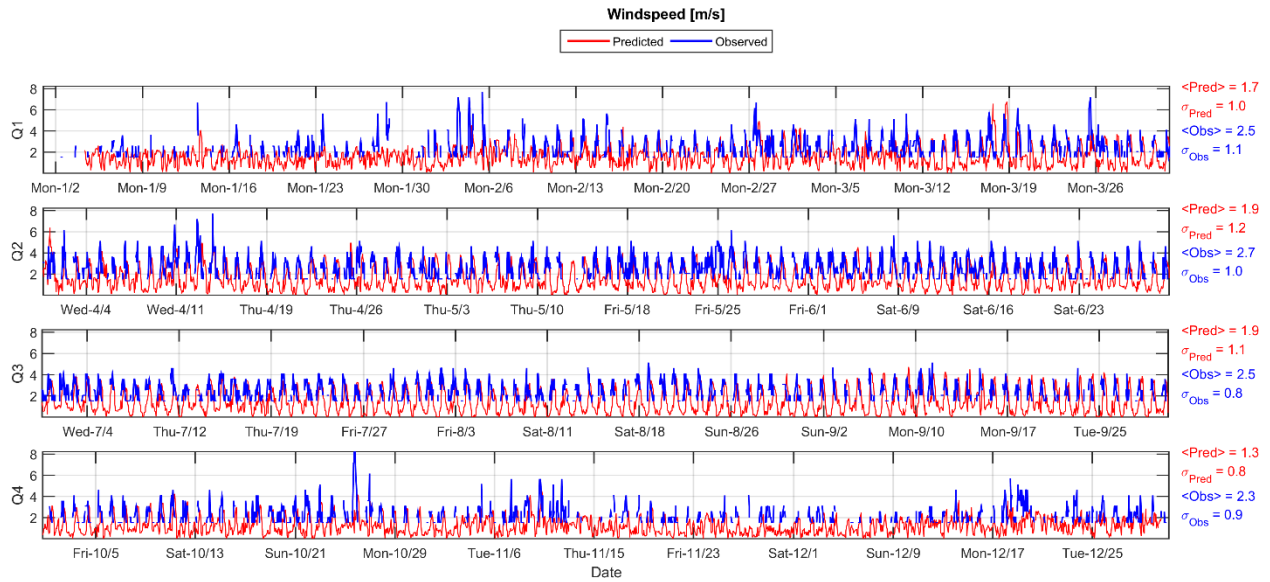


Figure S17: Yearly time series of wind speed observations and predictions in Fullerton

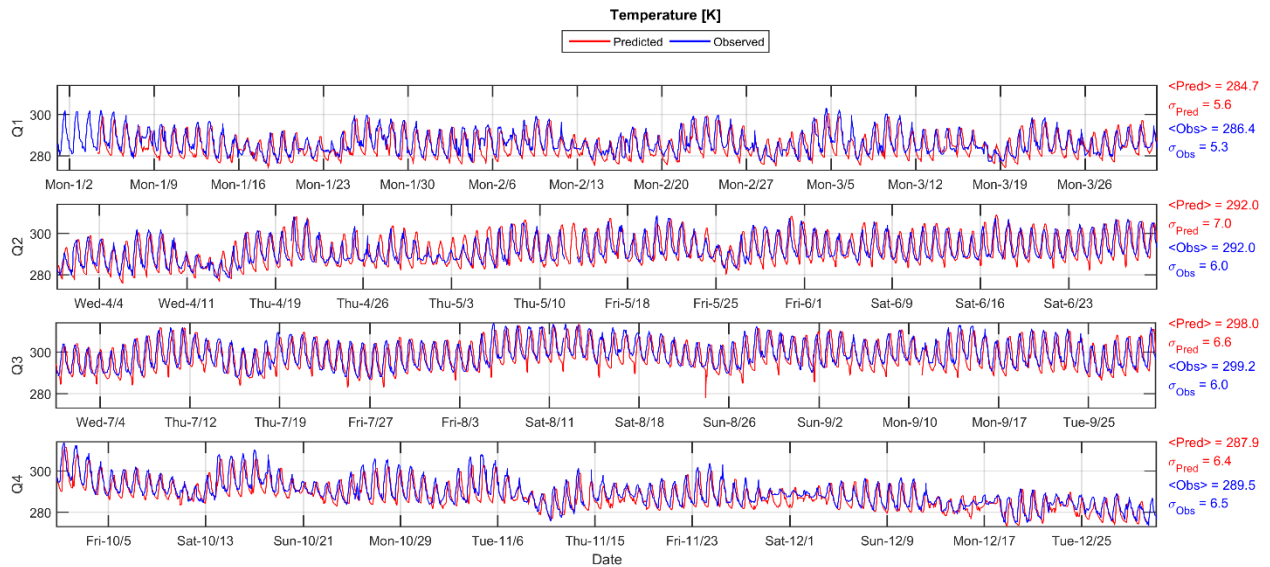


Figure S18: Yearly time series of temperature observations and predictions in Ontario

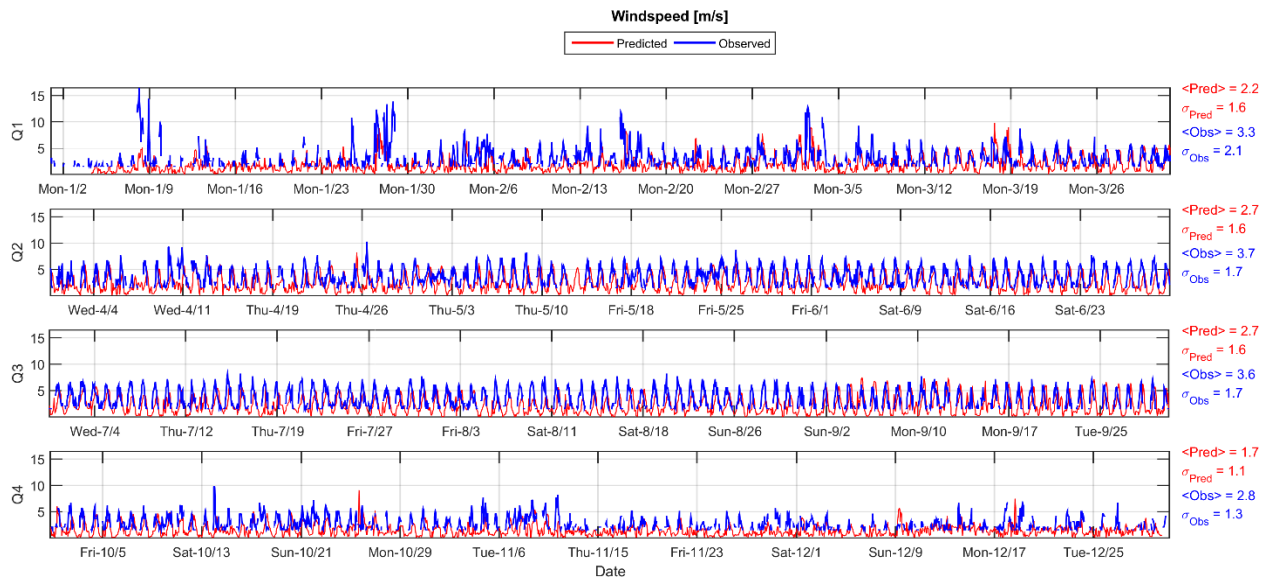


Figure S19: Yearly time series of wind speed observations and predictions in Ontario

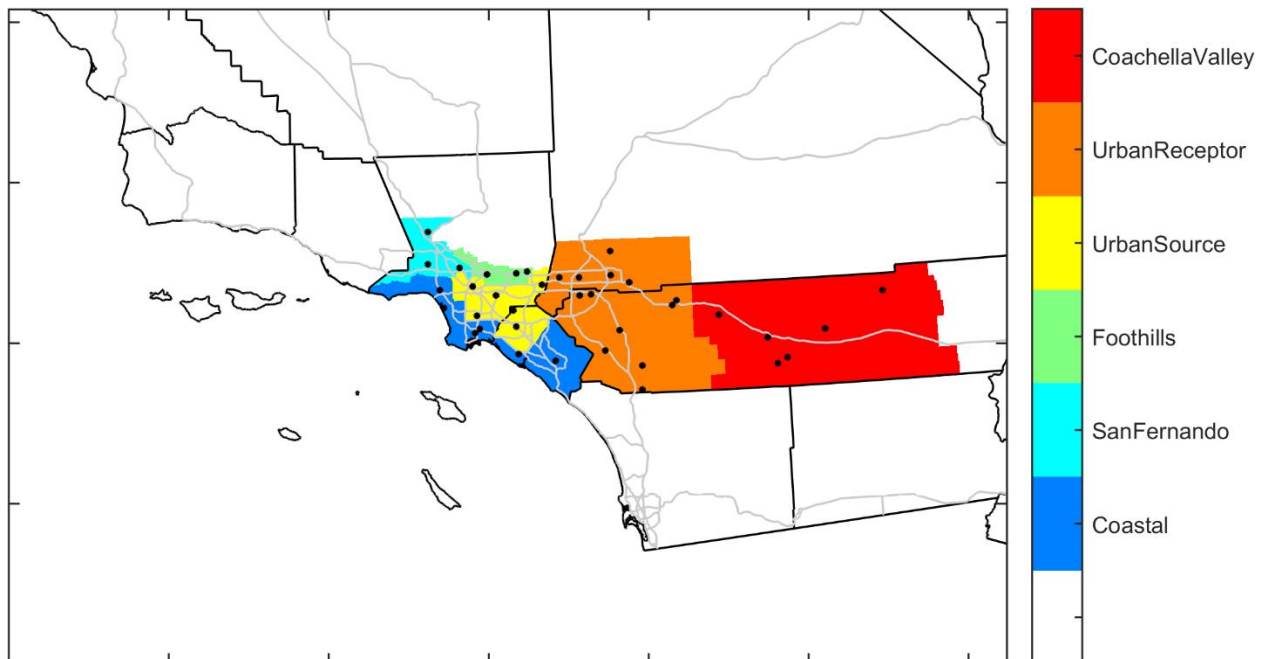


Figure S20: Ozone model performance regions in the South Coast Air Basin. Black circles indicate the locations of monitoring stations equipped with ozone monitors

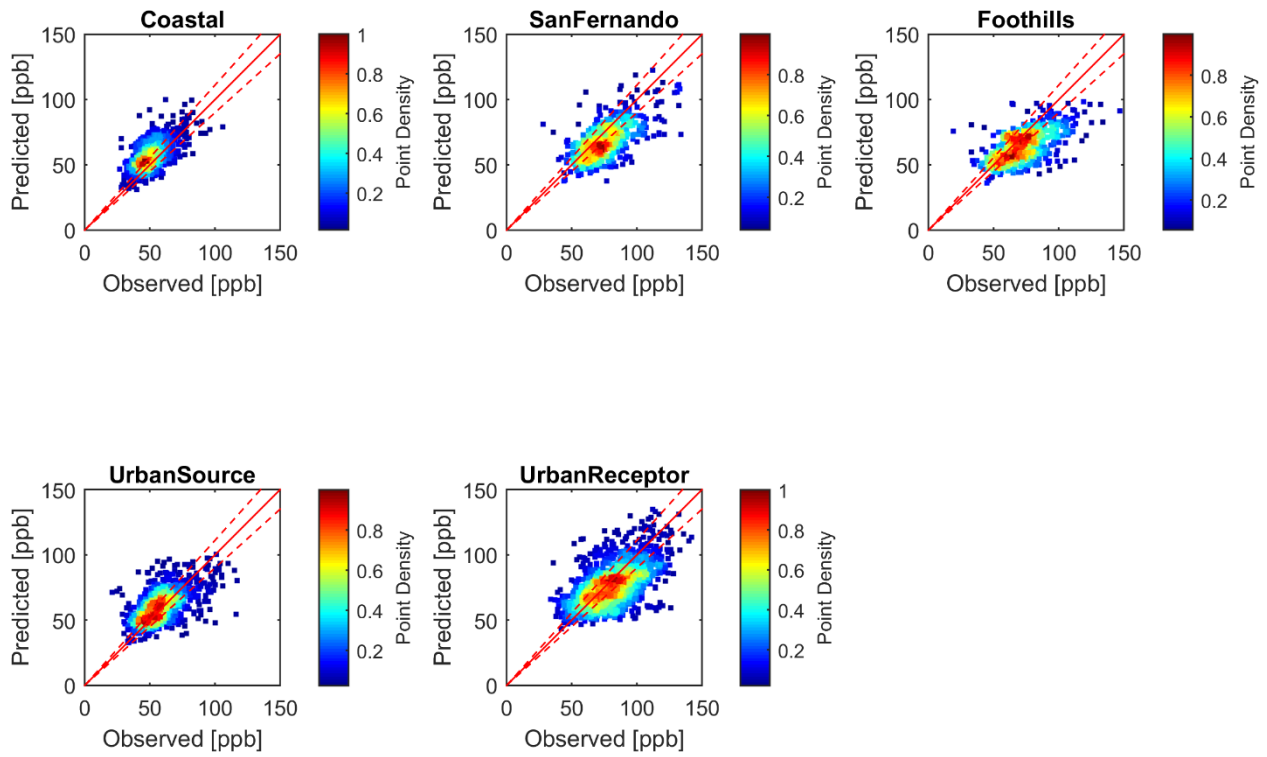


Figure S21: One-hour daily maximum ozone density scatter plots for each region in the Basin

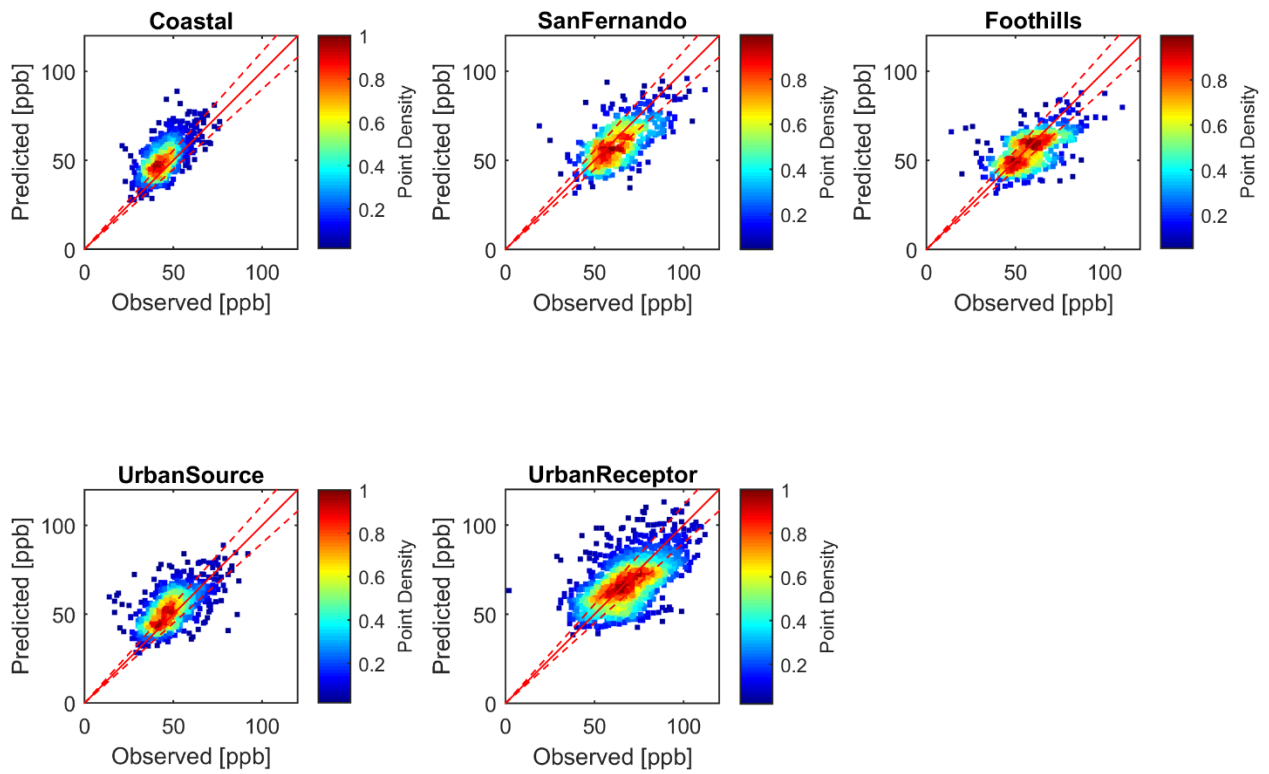


Figure S22: Eight-hour daily maximum ozone density scatter plots for each region in the Basin for 2012

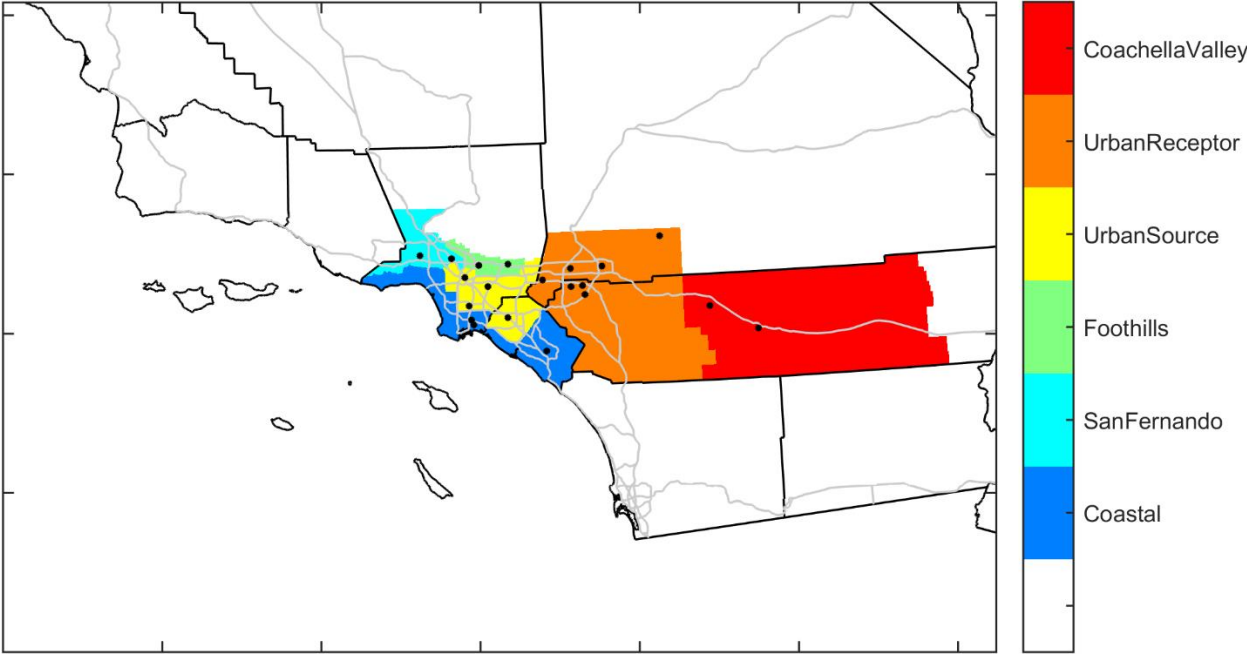


Figure S23: PM_{2.5} model performance regions. Black markers indicate the location of PM_{2.5} monitoring stations.

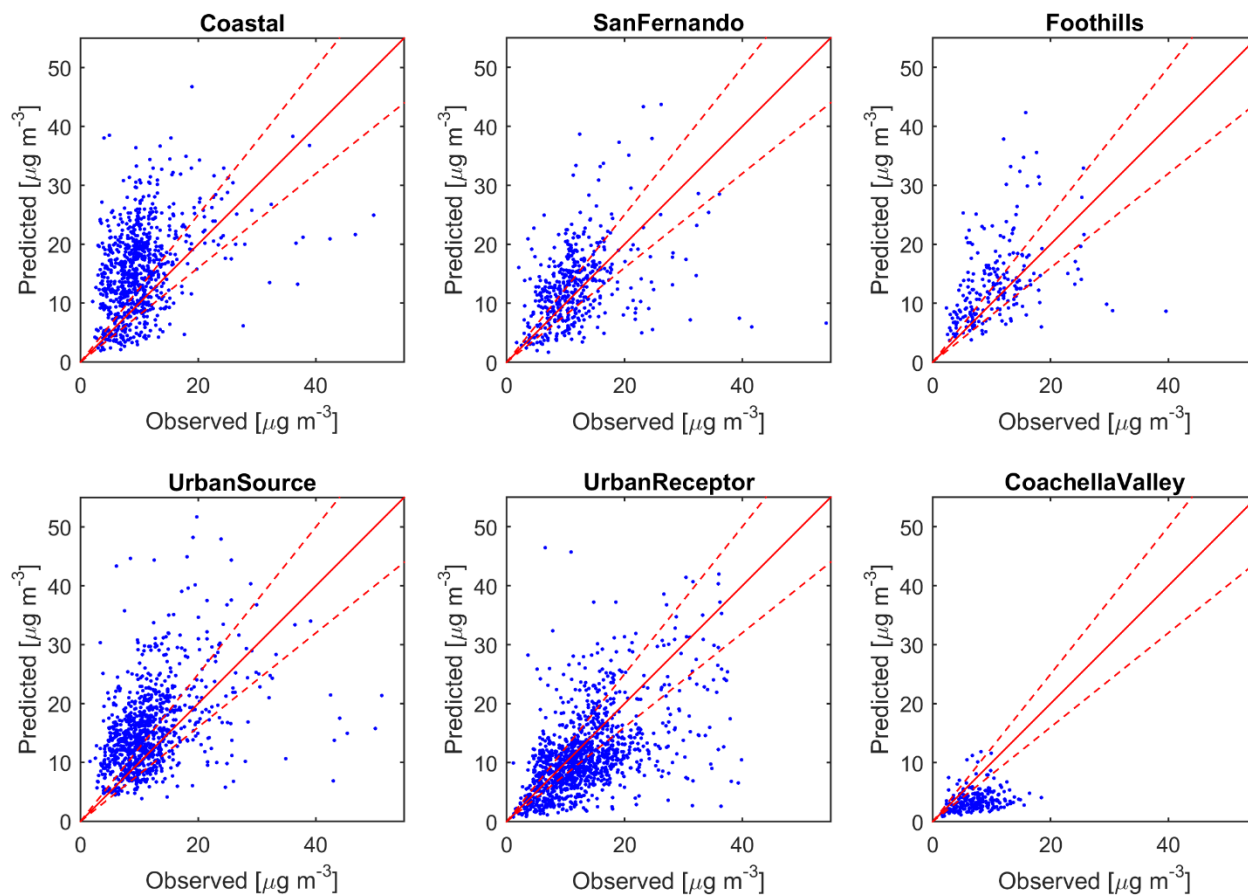


Figure S24: Comparison between predicted and observed daily-averaged $\text{PM}_{2.5}$ concentrations

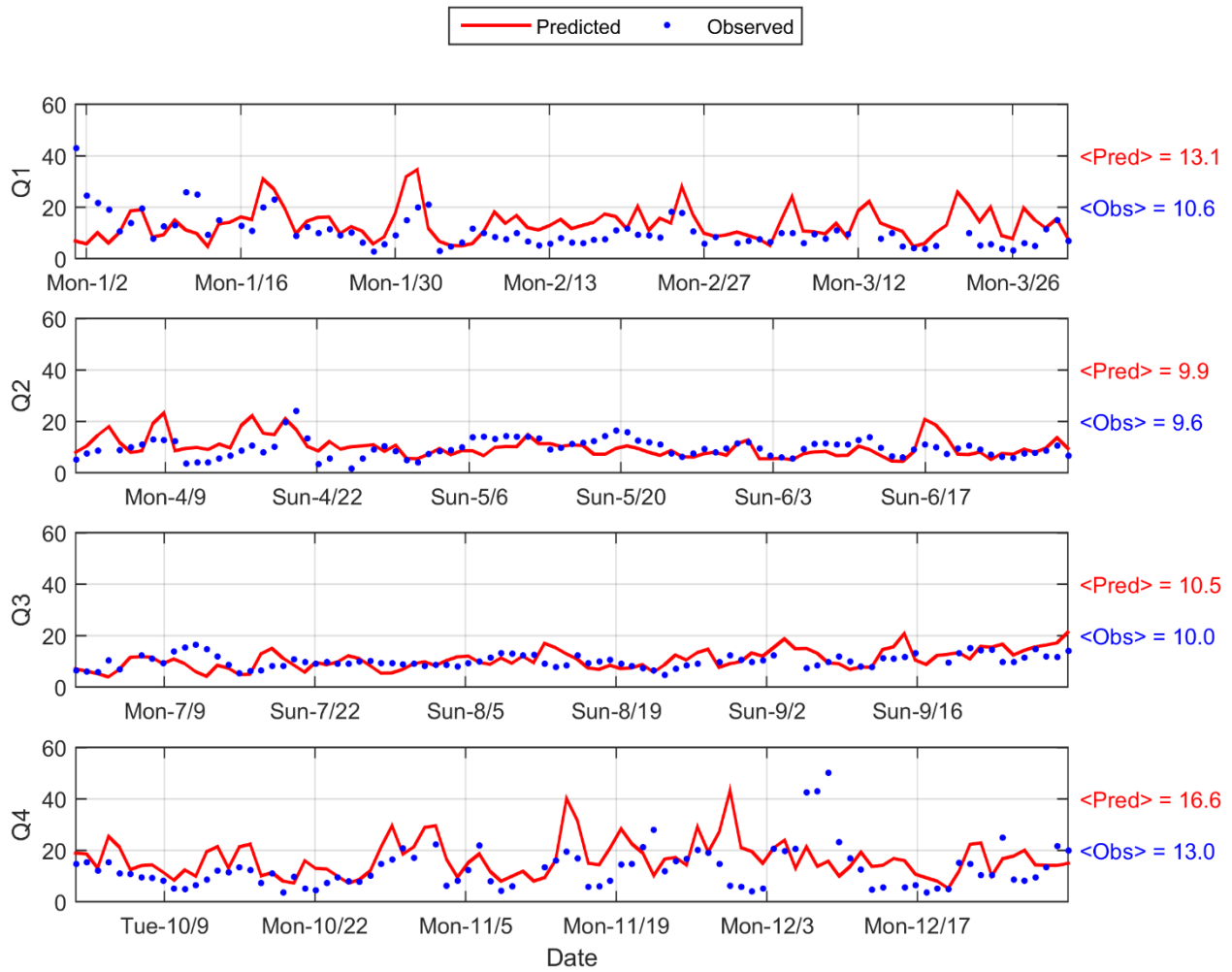


Figure S25: Time series of daily averaged PM_{2.5} predicted and observed concentrations in Anaheim

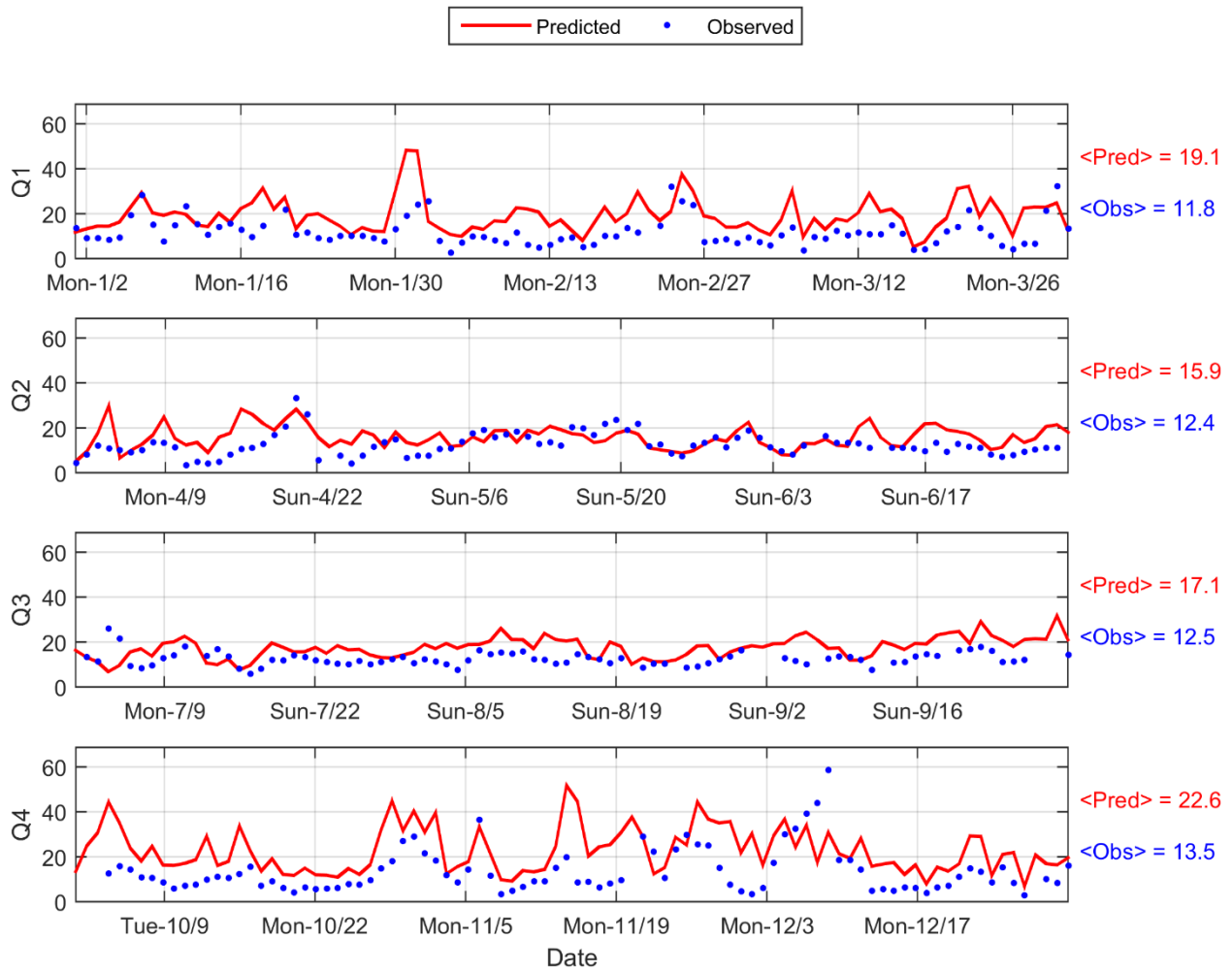


Figure S26: Time series of daily averaged PM_{2.5} predicted and observed concentrations in Central Los Angeles

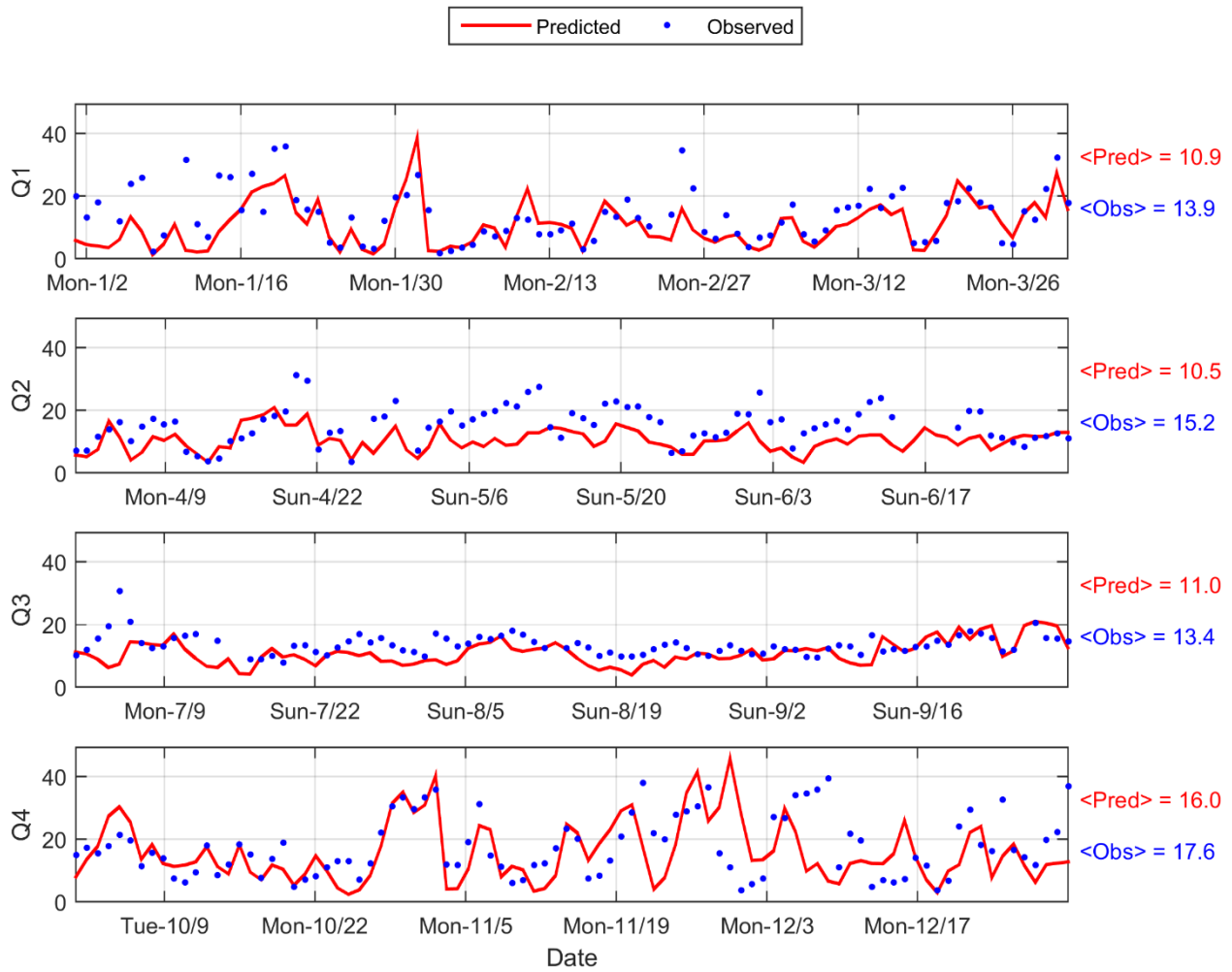


Figure S27: Time series of daily averaged PM_{2.5} predicted and observed concentrations in Mira Loma, the monitoring site with the highest PM_{2.5} concentrations in the Basin

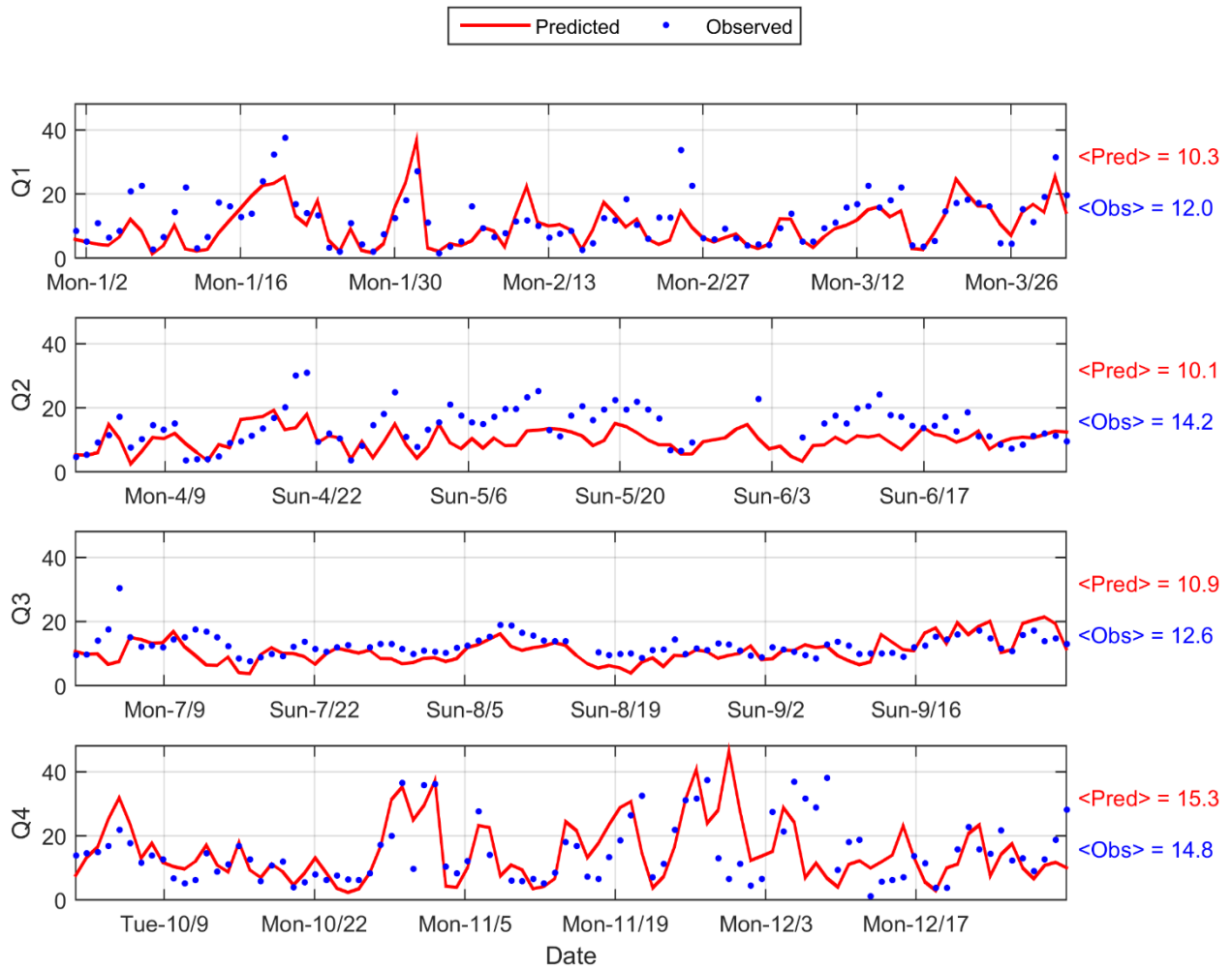


Figure S28: Time series of daily averaged PM_{2.5} predicted and observed concentrations in Riverside

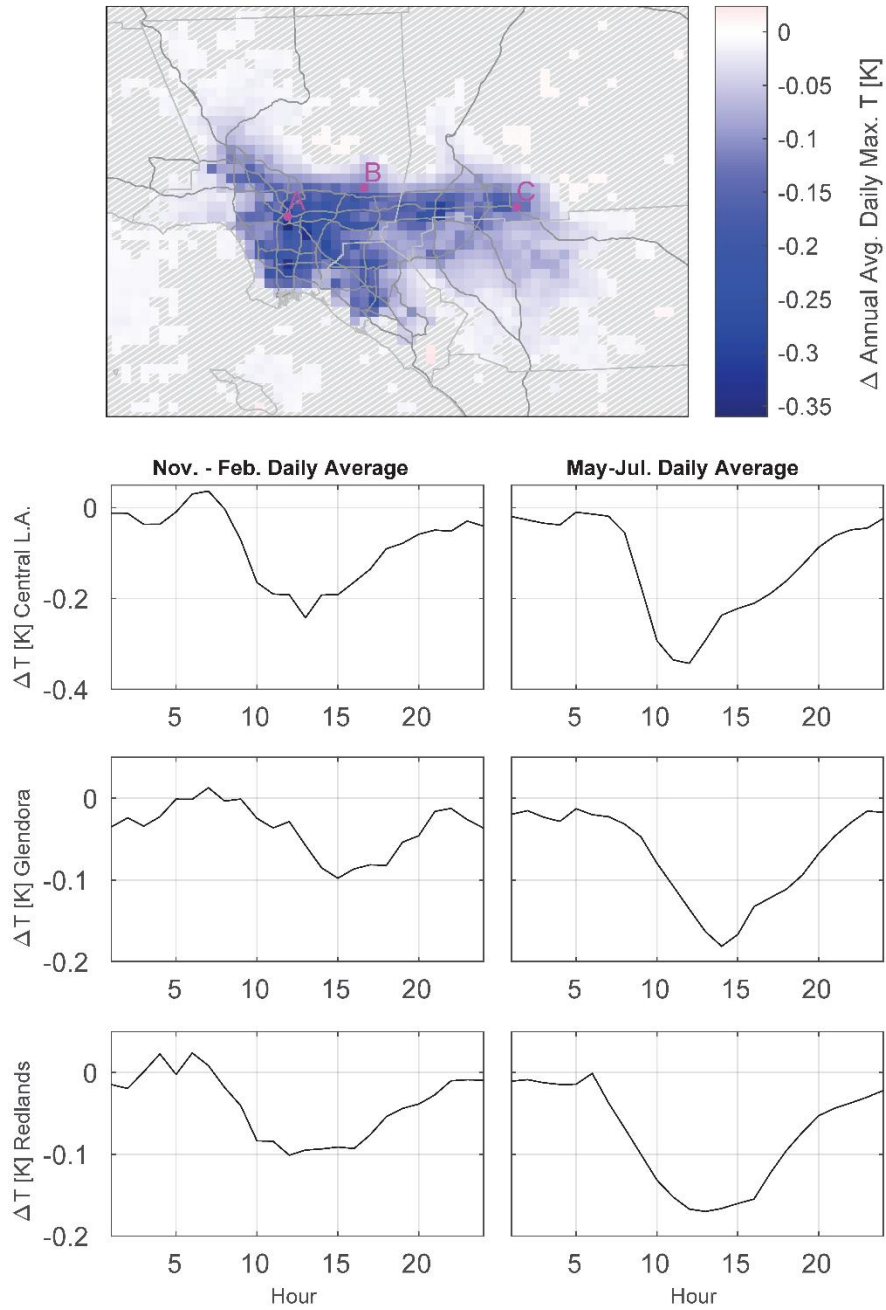


Figure S29: Difference in temperature (Title24 – Baseline) for each hour of the day at three locations across the Basin. Grey hashed cells indicate that differences are not statistically significant ($p > 0.05$).

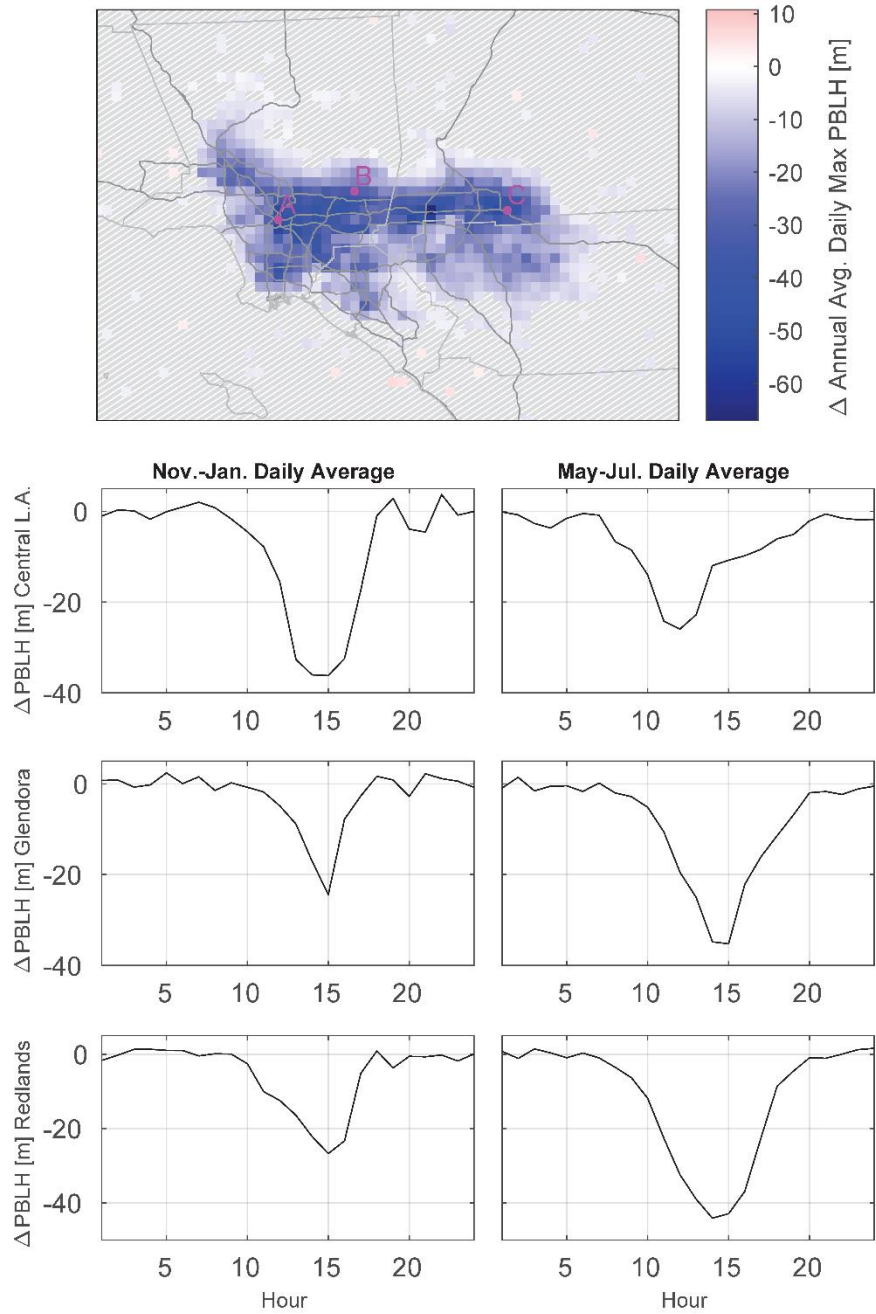


Figure S30: Difference in planetary boundary layer height (Title24 – Baseline) for each hour of the day at three locations across the Basin. Grey hashed cells indicate that differences are not statistically significant ($p > 0.05$).

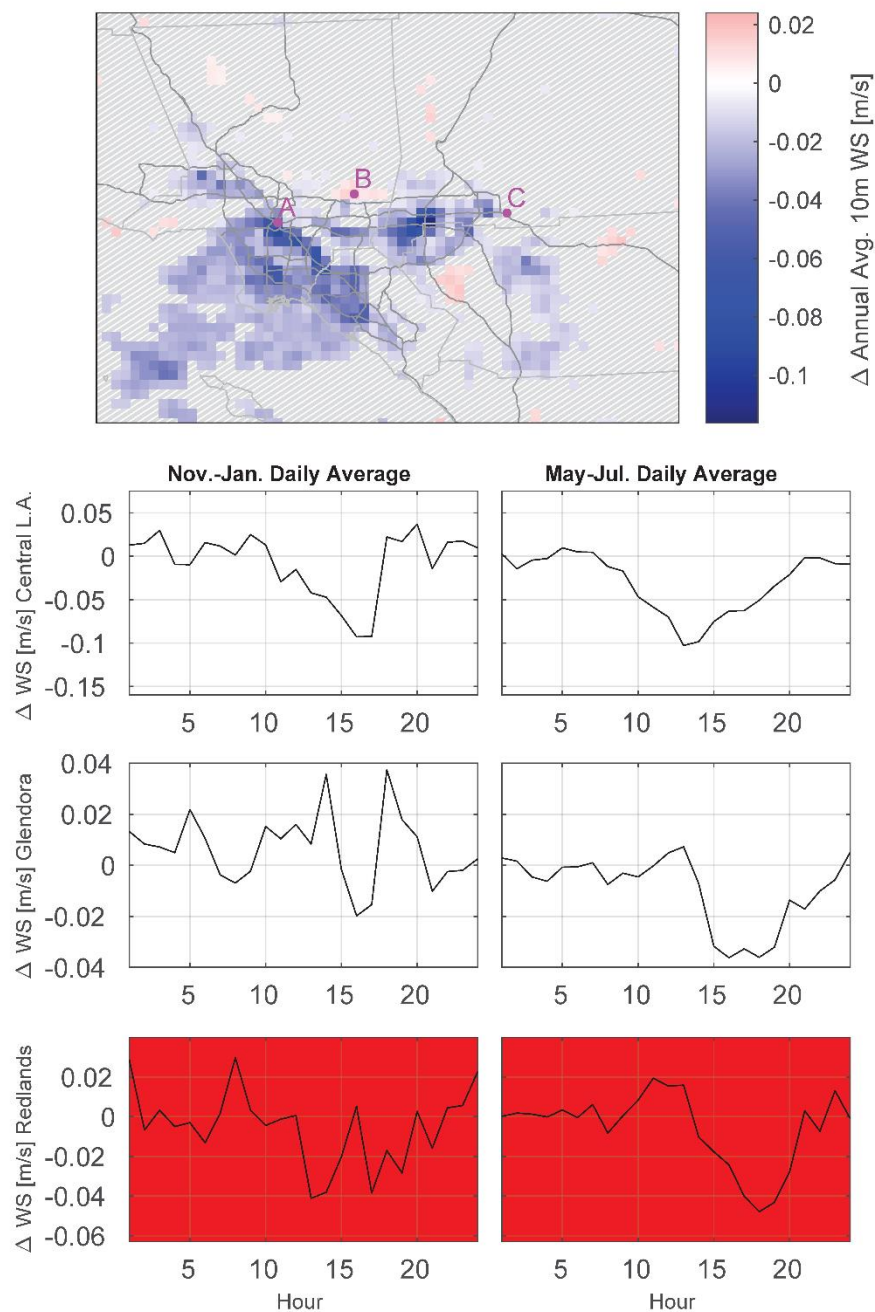


Figure S31: Difference in annual averaged 9am to 3 pm 10 m wind speed (Title24 – Baseline) for each hour of the day at three locations across the Basin. Grey hashed cells indicate that differences are not statistically significant ($p > 0.05$). Seasonal profiles in Redlands are highlighted in red because seasonal differences in wind speed are not statistically significant ($p > 0.05$) at that location.

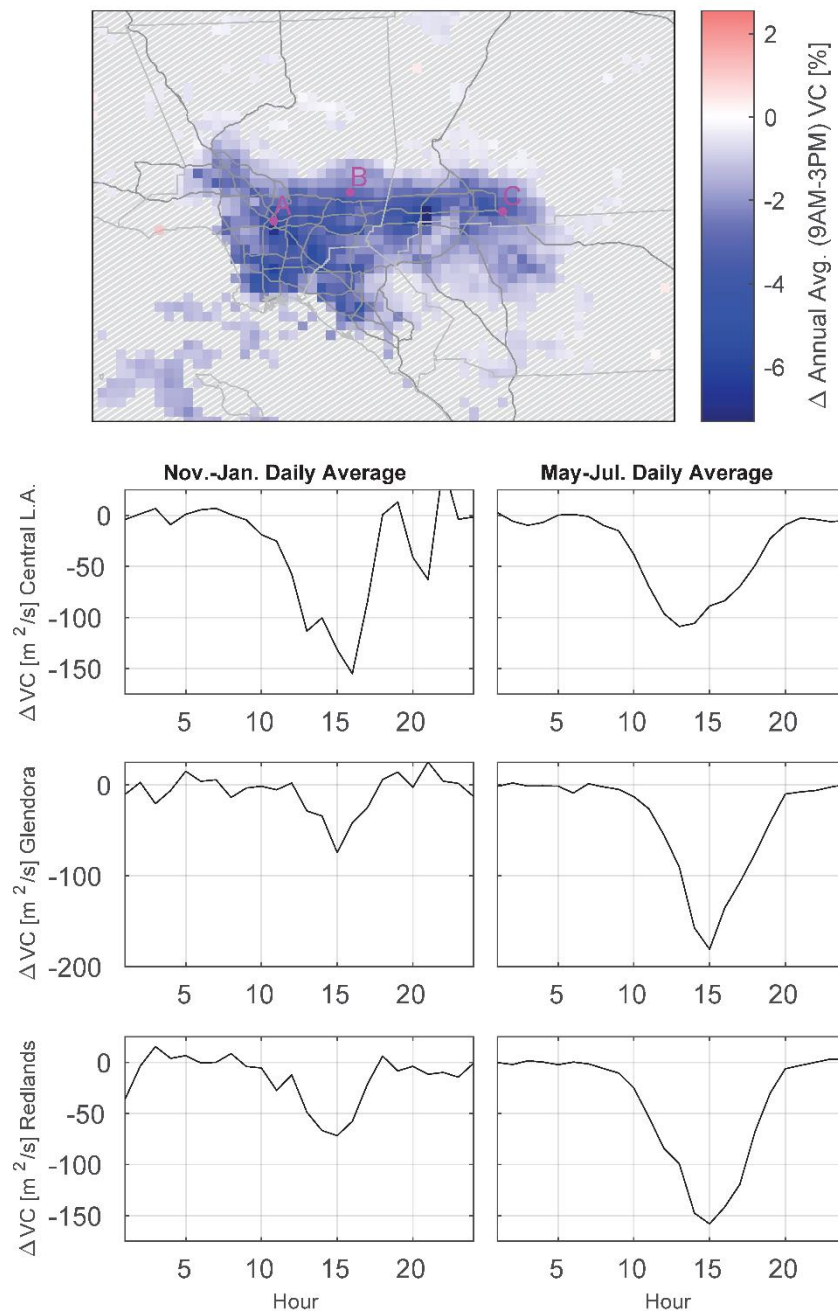


Figure S32: Difference in annual maximum ventilation coefficient (Title24 – Baseline) for each hour of the day at three locations across the Basin. Grey hashed cells indicate that differences are not statistically significant ($p > 0.05$).

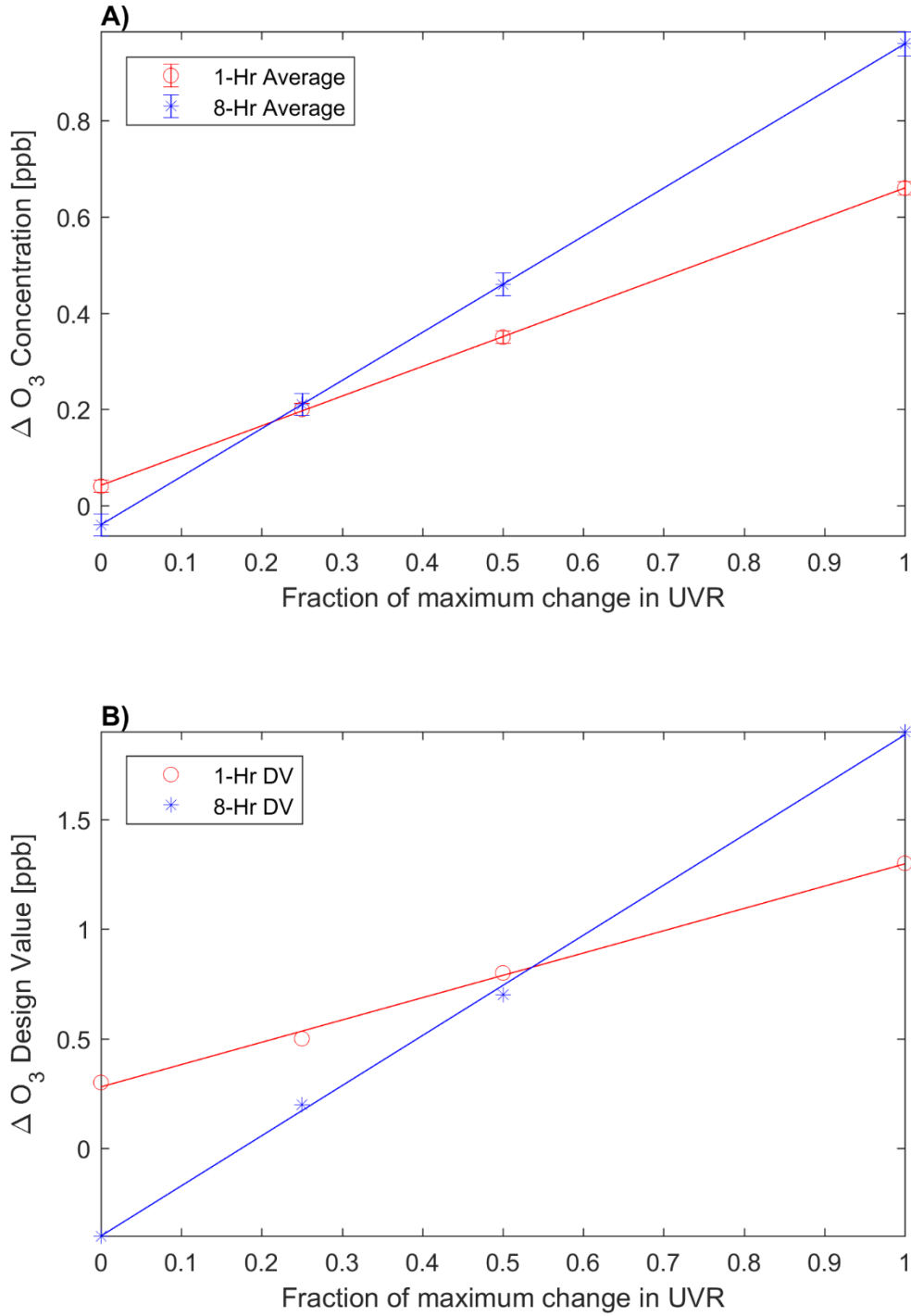


Figure S33: A) Change in ozone season average daily maximum 8-hour and 1-hour ozone concentrations at Redlands (Title24-Baseline) as the fractional change in UVR is varied from 0 (no change) to 1 (maximum change). B) Corresponding change in ozone design values.

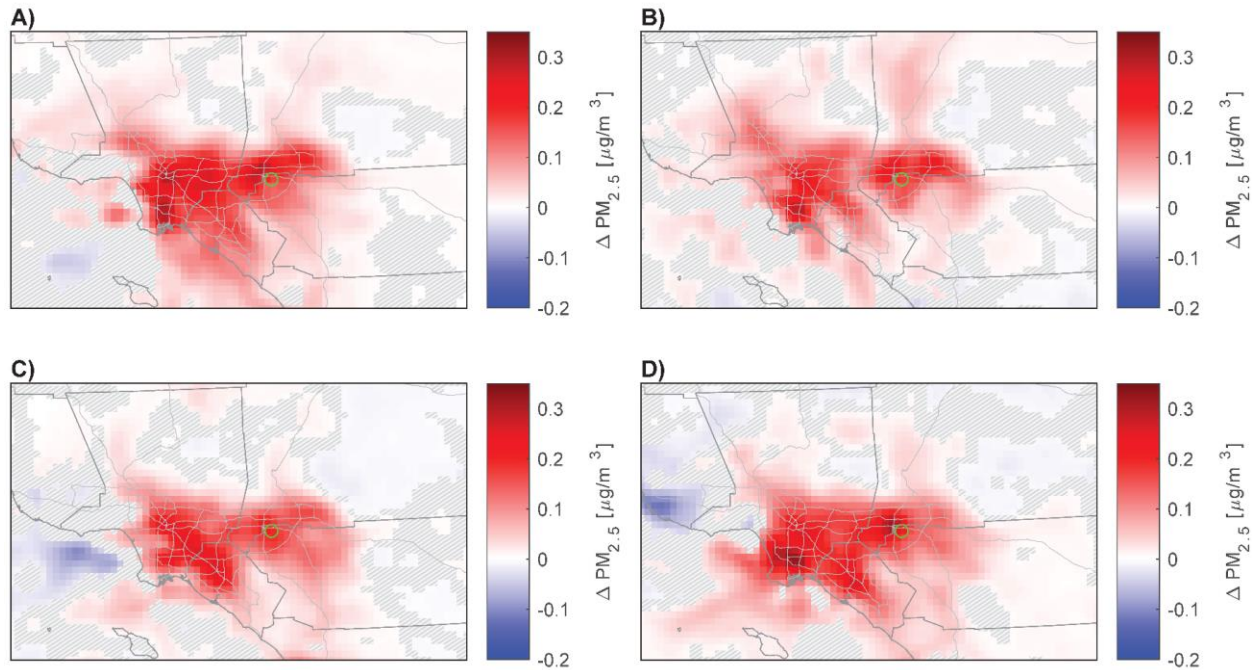
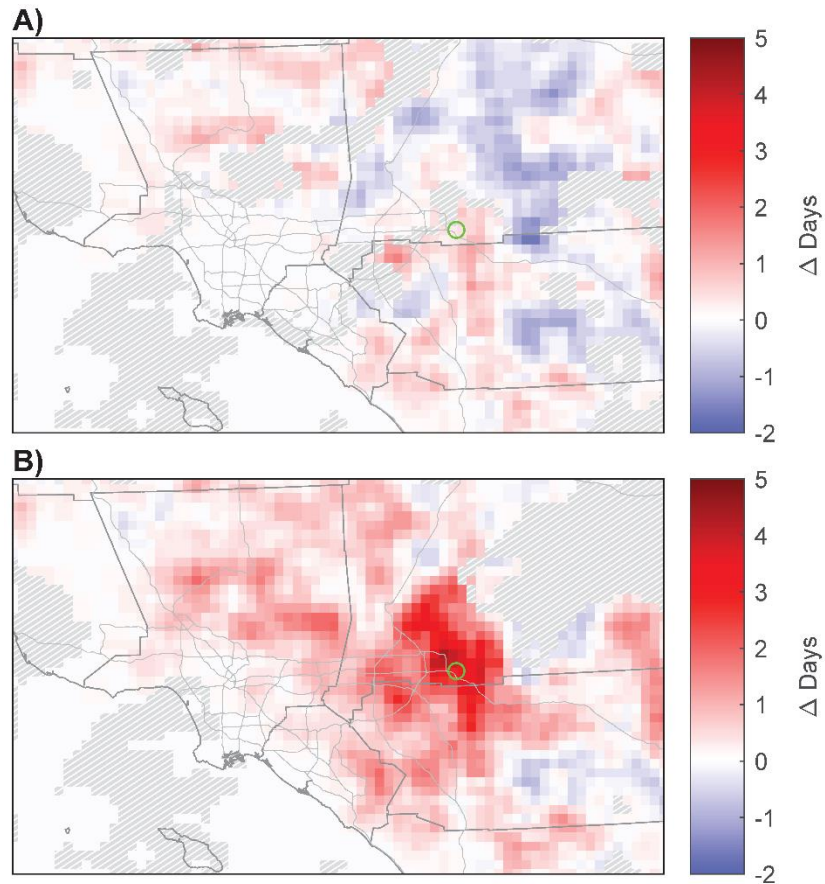


Figure S34: **A)** Average change in winter PM_{2.5} concentrations. **B)** Average change in spring PM_{2.5} concentrations. **C)** Average change in summer PM_{2.5} concentrations. **D)** Average change in autumn PM_{2.5} concentrations. Grey hashed cells indicate areas where changes are not statistically significant ($p > 0.05$). Image represents 3x3 cell moving average. Changes are largest in the winter and autumn months.



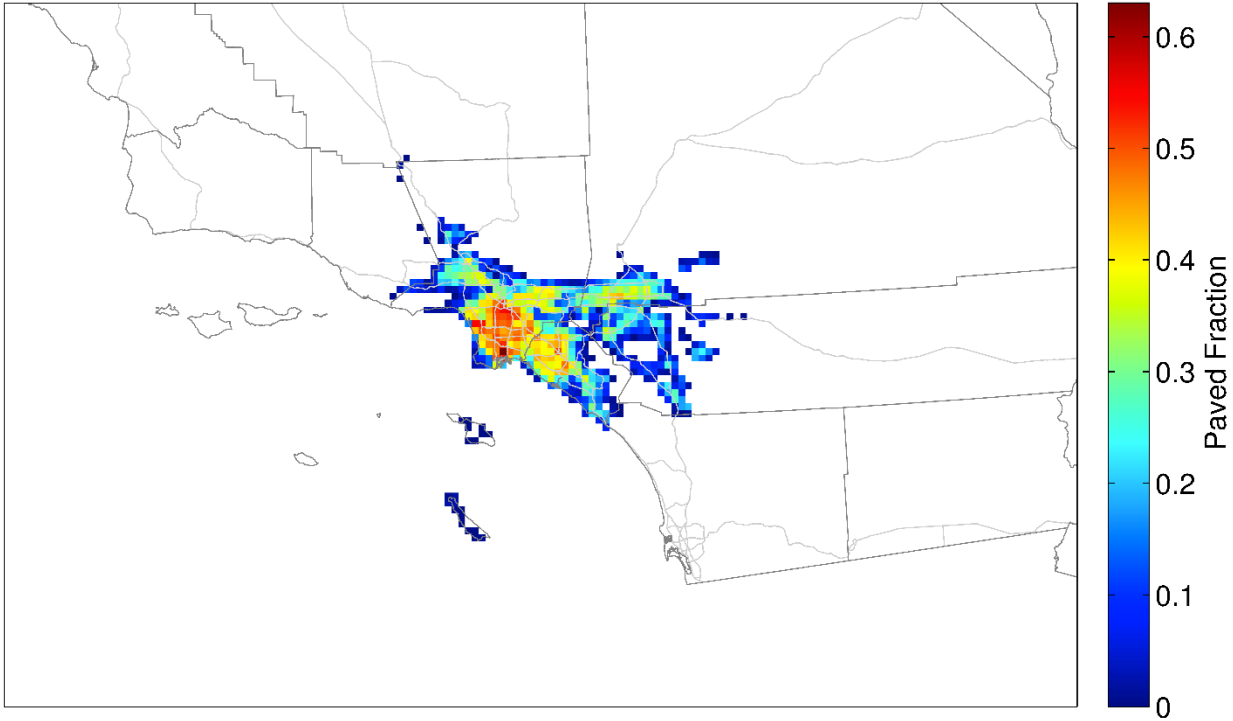


Figure S36: Fraction of each grid cell that is paved